



LRP10 and α -synuclein transmission in Lewy body diseases

Ana Carreras Mascaró¹ · Martyna M. Grochowska¹ · Valerie Boumeester¹ · Natasja F. J. Dits² · Ece Naz Bilgiç¹ · Guido J. Breedveld¹ · Leonie Vergouw³ · Frank Jan de Jong³ · Martin E. van Royen⁴ · Vincenzo Bonifati¹ · Wim Mandemakers¹

Received: 27 June 2023 / Revised: 13 January 2024 / Accepted: 21 January 2024
© The Author(s) 2024

Abstract

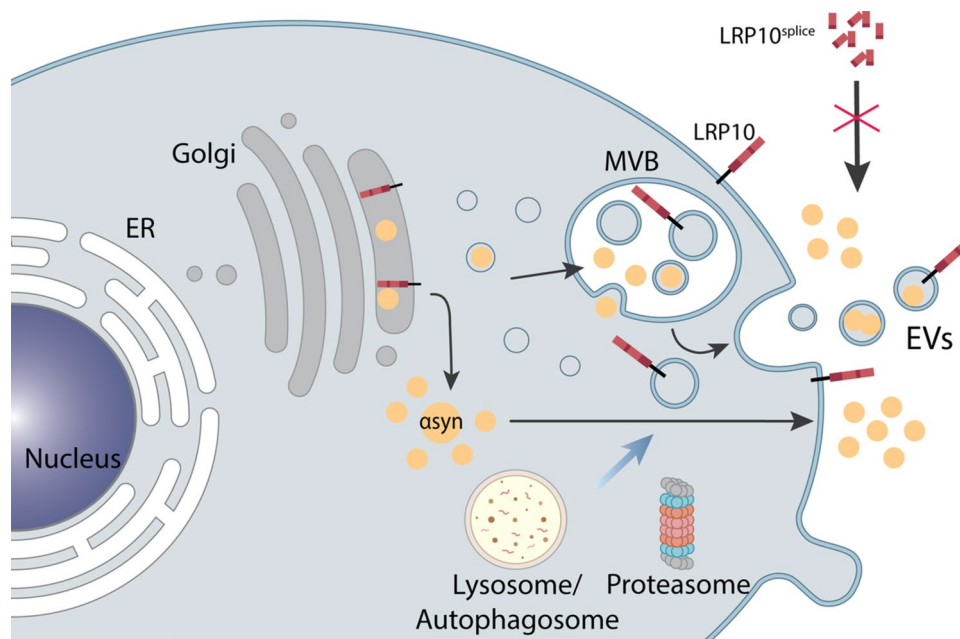
Autosomal dominant variants in *LRP10* have been identified in patients with Lewy body diseases (LBDs), including Parkinson's disease (PD), Parkinson's disease-dementia (PDD), and dementia with Lewy bodies (DLB). Nevertheless, there is little mechanistic insight into the role of LRP10 in disease pathogenesis. In the brains of control individuals, LRP10 is typically expressed in non-neuronal cells like astrocytes and neurovasculature, but in idiopathic and genetic cases of PD, PDD, and DLB, it is also present in α -synuclein-positive neuronal Lewy bodies. These observations raise the questions of what leads to the accumulation of LRP10 in Lewy bodies and whether a possible interaction between LRP10 and α -synuclein plays a role in disease pathogenesis. Here, we demonstrate that wild-type LRP10 is secreted via extracellular vesicles (EVs) and can be internalised via clathrin-dependent endocytosis. Additionally, we show that LRP10 secretion is highly sensitive to autophagy inhibition, which induces the formation of atypical LRP10 vesicular structures in neurons in human-induced pluripotent stem cells (iPSC)-derived brain organoids. Furthermore, we show that LRP10 overexpression leads to a strong induction of monomeric α -synuclein secretion, together with time-dependent, stress-sensitive changes in intracellular α -synuclein levels. Interestingly, patient-derived astrocytes carrying the *c.1424 + 5G > A* *LRP10* variant secrete aberrant high-molecular-weight species of LRP10 in EV-free media fractions. Finally, we show that this truncated patient-derived LRP10 protein species (LRP10^{splice}) binds to wild-type LRP10, reduces LRP10 wild-type levels, and antagonises the effect of LRP10 on α -synuclein levels and distribution. Together, this work provides initial evidence for a possible functional role of LRP10 in LBDs by modulating intra- and extracellular α -synuclein levels, and pathogenic mechanisms linked to the disease-associated *c.1424 + 5G > A* *LRP10* variant, pointing towards potentially important disease mechanisms in LBDs.

Martyna M. Grochowska and Valerie Boumeester Contributed equally.

✉ Wim Mandemakers
w.mandemakers@erasmusmc.nl

- ¹ Department of Clinical Genetics, Erasmus Medical Center, Rotterdam, The Netherlands
- ² Department of Urology, Erasmus Medical Center, Rotterdam, The Netherlands
- ³ Department of Neurology, Erasmus Medical Center, Rotterdam, The Netherlands
- ⁴ Department of Pathology, Erasmus Medical Center, Rotterdam, The Netherlands

Graphical abstract



Keywords Lewy body diseases (LBDs) · Parkinson's disease (PD) · Dementia with Lewy bodies (DLB) · Low-density lipoprotein receptor-related protein 10 (LRP10) · α -Synuclein · Extracellular vesicles (EVs) · Induced pluripotent stem cells (iPSC) · Astrocytes · Brain organoids

Abbreviations

AA	Ascorbic acid	GDNF	Glial cell line-derived neurotrophic factor
AD	Alzheimer's disease	GFAP	Glial fibrillary acidic protein
APP	Amyloid precursor protein	gRNA	Guide RNA
AQP4	Aquaporin 4	HEK-293T	Human embryonic kidney 293T
AU	Arbitrary Units	HUES	Human embryonic stem cell lines
BafA1	Bafilomycin A1	ICC	Immunocytochemistry
BDNF	Brain-derived neurotrophic factor	iPSCs	Induced pluripotent stem cells
BFA	Brefeldin A	IRES	Internal ribosome entry site
BSA	Bovine serum albumin	KO	Knock-out
CNTF	Ciliary neurotrophic factor	LBDs	Lewy body diseases
CQ	Chloroquine	LDLR	Low-density lipoprotein receptor
CSF	Cerebrospinal fluid	LRP10	Low-density lipoprotein receptor-related protein 10
C-t	C-terminal	NeoR	Neomycin resistance gene
dbcAMP	Dibutyryl cyclic adenosine monophosphate	NPCs	Neural precursor cells
DLB	Dementia with Lewy bodies	N-t	N-terminal
DMEM	Dulbecco's modified eagle medium	NTA	Nanoparticle tracking analysis
DMSO	Dimethylsulfoxid	PAGE	Polyacrylamide gel electrophoresis
DTT	Dithiothreitol	PBS	Phosphate buffered saline
EGF	Epidermal growth factor	PD	Parkinson's disease
ER	Endoplasmic reticulum	PDD	Parkinson's disease dementia
EVs	Extracellular vesicles	PFA	Paraformaldehyde
FBS	Fetal bovine serum	PuroR	Puromycin resistance gene
FGF	Fibroblast growth factor	QKI-7	Quakin 7
GBA	Glucosylceramidase		

RT-qPCR	Reverse transcription quantitative real-time PCR
SAG	Smoothed agonist
SDS	Sodium dodecylsulfate
SORL1	Sortilin-related receptor 1
TBS	Tris buffered saline
TEM	Transmission electron microscopy
TGF- β 3	Transforming growth factor beta 3
TH	Tyrosine hydroxylase
WB	Western blot
WT	Wild-type

Introduction

Lewy body diseases (LBDs) are neurodegenerative disorders characterised by the widespread presence of insoluble α -synuclein-containing aggregates, accompanied by the loss of dopaminergic neurons in the substantia nigra pars compacta [1]. The main LBDs include Parkinson's disease (PD), Parkinson's disease-dementia (PDD), and dementia with Lewy bodies (DLB), which collectively affect over 8 million people worldwide [2, 3]. PD, PDD, and DLB display overlapping clinical features that can include parkinsonian motor signs and cognitive impairment. The main distinction in their diagnosis is based on the temporal sequence of the onset of these symptoms. In addition to sharing many clinical and neuropathological features, LBDs also present shared genetic factors, such as *GBA1*, *SNCA*, and *LRP10* genetic variants [4–9].

The low-density lipoprotein receptor (LDLR)-related protein 10 (LRP10) is a single-pass transmembrane protein and a member of the LDLR family [10]. LRP10 function has been linked to the intracellular vesicle transport pathway due to its intracellular localisation pattern and interaction with clathrin adaptors and the retromer complex [9, 11–15]. Increasing genetic and neuropathological evidence has positioned LRP10 as a novel player in LBDs. Several studies have identified potentially pathogenic variants in the encoding gene *LRP10* in autosomal dominant forms of PD, PDD, and DLB [9, 16–23]. Furthermore, recent work from Grochowska et al. [11] showed that 71 to 95% of mature brainstem Lewy bodies in ten patients suffering from idiopathic and genetic cases of PD, PDD, and DLB were strongly positive for LRP10, even though its expression was almost limited to astrocytes and neurovasculature in control brains. Besides LBDs, *LRP10* variants were also identified in patients with progressive supranuclear palsy and amyotrophic lateral sclerosis [24, 25]. Furthermore, LRP10 function has been associated with Alzheimer's disease (AD). In addition to its physical interaction with SORL1, LRP10 has been described to be a receptor for the amyloid precursor protein (APP) and ApoE-carrying lipoproteins, and it has

been shown to be a driver of an AD subtype [11, 26–28]. Despite this effort, LRP10 function and its implication in neurodegeneration remain incompletely characterised.

The deposition of α -synuclein aggregates is a defining pathological feature of LBDs, and the cell-to-cell transmission of α -synuclein pathology is considered a major player in the disease progression [29]. α -Synuclein is a presynaptic protein that is normally found in a soluble cytosolic state or bound to cellular membranes [30–33]. However, several forms of α -synuclein have been associated with increased misfolding and aggregation potential, including the acquisition of a β -sheet amyloid conformation, post-translational modifications, and genetic variations [32, 34]. The factors triggering the misfolding and deposition of α -synuclein in the human brain are still not clear, and they may vary per patient, affected brain area, and disease [35]. In contrast, the transmission of soluble and pathological α -synuclein is well established, and it has been identified on the cellular level but also between anatomically connected brain areas and between the brain and other organs, such as the gastrointestinal tract and peripheral muscles [36–43].

Based on these observations, we aimed to investigate whether the presence of LRP10 in Lewy bodies could be caused by the transfer of LRP10 from non-neuronal cells and subsequent internalisation by dopaminergic neurons, and whether LRP10 may play a role in regulating α -synuclein in LBD pathogenesis. Using human-induced pluripotent stem cells (iPSC)-derived brain organoids, astrocytes, and LRP10-overexpressing cells as model systems, we found that LRP10 can be secreted via extracellular vesicles (EVs) and is highly sensitive to autophagy blockade by Bafilomycin A1 (BafA1), which induced the formation of atypical LRP10 structures in neurons in brain organoids. Additionally, we found that LRP10 overexpression induces changes in α -synuclein intracellular levels over time, and strongly promotes α -synuclein secretion via the endoplasmic reticulum (ER) and proteasomal pathways. Lastly, we show that the *LRP10 c.1424+5G>A* genetic variant found in LBD patients [9] affects LRP10 secretion and internalisation and has a dominant negative effect on LRP10-mediated modulation of intra- and extracellular α -synuclein levels. Altogether, our results suggest a possible role for LRP10 as an α -synuclein modulator in LBDs.

Methods

Cloning

To generate the pLVX-EF1 α -LRP10-IRES-NeoR plasmid used for LRP10 overexpression, *LRP10* sequence-verified cDNA was subcloned from the pcDNATM3.1-LRP10-V5-His-TOPO[®] plasmid described previously

[9] into the pLVX-EF1 α -IRES-mCherry plasmid (Takara Bio, 631987). Briefly, LRP10 was inserted after the EF1 α promoter in EcoRI and BamHI-digested pLVX-EF1 α -IRES-mCherry using Gibson Assembly® (NEB) according to the manufacturer's specifications. Next, the backbone was purified after MluI and MscI digestion from gel using the QIAquick® Gel Extraction Kit (Qiagen) excluding mCherry. The Neomycin resistance gene (NeoR) was subcloned from the pcDNATM3.1-LRP10-V5-His-TOPO® plasmid and located in place of mCherry via Gibson Assembly®. The negative control plasmid pLVX-EF1 α -IRES-NeoR was generated by restriction digestion (EcoRI and BamHI), blunt end generation, and T4 ligation of pLVX-EF1 α -LRP10-IRES-NeoR. The pLVX-EF1 α -LRP10^{splice}-IRES-NeoR plasmid was generated by PCR of specific regions of LRP10 from the pLVX-EF1 α -LRP10-IRES-NeoR plasmid (LRP10^{splice} sequence can be found in Supplementary resource 1), and placed into the same plasmid after EcoRI, BamHI, BsmBI, and Xcm I restriction digestion to linearize the backbone and digest LRP10 wild-type, respectively.

The pcDNATM3.1-mCherry-LRP10 plasmid was generated from the pcDNATM3.1-LRP10-V5-His-TOPO® plasmid. Briefly, a stop codon was first introduced between LRP10 and V5-His sequences (described in detail in Quadri and Mandemakers, et al. [9]). Next, LRP10 was amplified by PCR introducing a BspEI restriction site at the N-terminal end of LRP10 and reintroduced into the same backbone by T4 ligation. Finally, mCherry was introduced into the pcDNATM3.1-BspEI-LRP10 plasmid via PCR amplification from the pmCherryN1 plasmid (Clontech) via the addition of BspEI restriction sites in the primer sequences, restriction digestion with BspEI, and T4 ligation.

To produce the plasmid used to generate LRP10 knock-out neuronal precursor cells (NPCs), pSpCas9-GFP-LRP10gRNA [11, 44] was digested with BseRI and BsrGI, and GFP was replaced with Puromycin resistance gene (PuroR, subcloned from GIPZ Non-silencing Lentiviral shRNA Control, Horizon, RHS4346) via Gibson Assembly®, resulting in the pSpCas9-PuroR-LRP10gRNA plasmid.

The pCMVSPORT6-SNCA (Horizon, clone Id: 6147966) plasmid was used for α -synuclein overexpression experiments.

To generate the doxycycline-inducible LRP10^{splice} cell line, the pCW57-LRP10^{splice}-2A-PuroR was used. First, LRP10^{splice} was subcloned from the pLVX-EF1 α -LRP10^{splice}-IRES-NeoR plasmid via PCR and placed after the rtTA (reverse tetracycline-controlled transactivator)-Advanced promoter in the AgeI-digested pCW57-MCS1-2A-MCS2 (Addgene, 71782, from Adam Karpf) plasmid via Gibson Assembly®. All plasmids were verified by Sanger sequencing.

HEK-293T and HuTu-80 cell culture and transfection

HEK-293T and HuTu-80 (CLS, 300,218) cell lines were expanded in growth medium (DMEM or DMEM:F12, respectively; Thermo Fisher Scientific, 10% fetal bovine serum (FBS), 1% Penicillin–Streptomycin) at 37 °C/5% CO₂. Cells were split every 2–3 days with Trypsin–EDTA (Gibco). Prior to transfection, HEK-293T cells were seeded to a 60–70% confluency in tissue culture plates. Transfections were performed using the GeneJuice® transfection reagent (Merck) according to the manufacturer's specifications, and the samples were further processed 48 h after transfection or when specified.

Primary cell lines

Details regarding the primary cell lines used in this study can be found in Table 1. The Control-1 cell line was obtained from the Gladstone Institutes. The Control-3 line was commercially available (Gibco). The Control-2 cell line and the line derived from the DLB patient carrying the *LRP10* c.1424+5G>A variant [9] were obtained within study protocols approved by the medical ethical committee of Erasmus MC and conformed to the principles of the Declaration of Helsinki. The participating subjects provided written informed consent for the use of the material for research purposes and publication. The human embryonic stem cell lines (HUES) used in the RT-qPCR experiments (Supplementary Fig. 5) were a kind gift

Table 1 Details of the control and patient clonal lines included in this study

Donor	Source	Donor age	Donor sex	Donor sampling site	Derivation
Control-1	WTC, Gladstone Institutes (Coriell Research Institute, GM25256)	30	Male	Dermal fibroblasts	Brain organoids and astrocytes; LRP10 knock-out (LRP10 ^{KO}) astrocyte line
Control-2	In house	57	Male	Dermal fibroblasts	Astrocytes
Control-3	Gibco TM , Lot number: 18388	34	Female	Dermal fibroblasts	Brain organoids
DLB Patient	In house	68	Female	Dermal fibroblasts	Clones 1 and 2—astrocytes Clone 3—brain organoids

from Chad A. Cowan (Harvard University, Harvard Stem Cell Institute) [45].

Generation and characterisation of human iPSCs

Control-1 was generated and characterised as previously described by Mandegar et al. [46]. Control-2 was reprogrammed and characterised as described earlier [9, 47]. Patient iPSCs were collected, and the total RNA was isolated using the ReliaPrep™ RNA MiniPrep kit (Promega) as recommended by the manufacturer. For each sample, on-membrane DNase I digestion was performed according to the manufacturer's protocol (Promega). The integrity of the total RNA was assessed using spectrophotometric analysis using NanoDrop 2000/2000c. 260/280 values of ~2.0 indicated pure RNA. Next, 2 μ g of the total RNA was converted into cDNA using the SuperScript II Reverse Transcriptase kit (Invitrogen™). qPCR was performed on CFX384 Real-Time PCR Detection System (Bio-Rad) with ~20 ng cDNA per reaction. The following cycling conditions were used: 3 min at 95 °C (initial denaturation), 40 cycles of 30 s at 95 °C, 30 s at 58 °C, and 72 s at 72 °C. The normalised expression of each target gene was calculated using the delta–delta C_q method. *GAPDH* was used as a reference gene. HUES 9 line was used for the normalisation of the gene expression. Primers were adapted from a previously published article [48].

Generation of neural progenitor cells

The procedure to generate neural progenitor cells (NPCs) was adapted from Reinhardt et al. [49] and is described in detail in Grochowska et al. [11]. Briefly, iPSCs were detached and cultured as embryoid bodies in suspension in a shaker. Neural induction was initiated by promoting Wnt and Shh signalling with the addition of SB431542 (Tocris, 1614), dorsomorphin (Abcam, ab120843), CHIR (Sigma-Aldrich, SML1046), and Purmorphamine (Stem Cell Technologies, 72,202). Embryoid bodies showing neuroepithelial development were selected, dissociated, and plated on Matrigel® (Corning, 356238)-coated plates as NPCs. From the sixth passage, NPCs were kept in NPC medium, consisting of N2B27 medium (DMEM/F-12—Neurobasal in 1:1 ratio, 1% B27 w/o Vitamin A, 0.5% N2, 1% Penicillin–Streptomycin, all from Thermo Fisher Scientific) supplemented with 3 μ M CHIR, 200 μ M ascorbic acid (AA, Sigma-Aldrich, A92902), and 0.5 μ M Smoothed Agonist (SAG, Abcam, ab142160). Cells were kept on Matrigel-coated plates, refreshed every other day, and split with accutase (Sigma-Aldrich) in a 1:10–1:20 ratio.

Astrocyte differentiation

NPCs were differentiated into astrocytes according to published protocols [11, 49] with minor modifications. First, 75,000 NPCs/cm² were seeded on Matrigel® (Corning)-coated plates with N2B27 medium supplemented with 10 ng/mL FGF-basic (PeproTech, 100-18B) and 10 ng/mL EGF (PeproTech, AF-100-15). After 2 days, this medium was switched to N2 medium (Advanced DMEM/F-12, 4% FBS, 1% N2, 1% Penicillin–Streptomycin) supplemented with 10 ng/mL CNTF (PeproTech, 450-13). After 12 days, cells were grown in N2 medium with 10 ng/mL EGF. At 2 months of differentiation, cells were frozen in N2 medium with 10% DMSO. All the lines were thawed simultaneously and kept in N2 medium with 10 ng/mL EGF for 2–3 weeks, followed by at least 10 days of N2 medium with 10 ng/mL CNTF. Cells were refreshed every other day. One week before terminating cultures, cells were treated with 100 μ M dbcAMP in N2 medium. Cells were cultured for at least 3 months. Astrocyte cultures were split with accutase (Sigma-Aldrich) at a 1:2–1:5 ratio when maximal density was reached, leaving most cell clumps intact.

Brain organoids differentiation

NPCs were differentiated into brain organoids according to published protocols [50, 51] with minor modifications. NPCs were dissociated with accutase (Sigma-Aldrich), briefly centrifuged, and resuspended in NPC medium. Cells were counted using the TC20 automated cell counter (Bio-Rad) and plated at a density of 9000 cells/well on BIOFLOAT™ 96-well plates (faCellitate, F202003). The plate was centrifuged at 220 \times g for 5 min and placed in the incubator at 37 °C/5% CO₂. After 48 h, the medium was switched to patterning medium (N2B27 supplemented with 200 μ M AA, 1 ng/mL BDNF (Prospec, CYT-207), 1 ng/mL GDNF (PeproTech, 450-10), and 1 μ M SAG). After 2 days, the brain organoid media was refreshed with patterning medium. After 2 days, the medium was replaced with maturation medium (N2B27 supplemented with 200 μ M AA, 2 ng/mL BDNF, 2 ng/mL GDNF, 1 ng/mL TGF- β 3 (Prospec, CYT-368), 5 ng/mL ActivinA (Stem Cell Technologies, 78001), and 100 μ M dbcAMP (Sigma-Aldrich, D0260). ActivinA concentration was lowered to 2 ng/mL for the subsequent media changes. The medium was changed every other day. On day 30, the medium was switched to N2B27 without supplements and refreshed every other day.

Drug treatments

The following reagents were added directly or mixed with growth medium, exosome-free growth medium, or DMEM and placed on cultured cells for the specified time points:

Bafilomycin A1 (BafA1, 200 nM, Enzo, BML-CM110-0100; Lactate Dehydrogenase (LDH) assay (CytoTox-ONE, G7891, Promega), procedure according to manufacturer's specifications), Torin1 (200 nM, Invivogen, inh-tor1), Methylamine hydrochloride (2 mM, Sigma-Aldrich, m0505), Chloroquine (CQ, 50 μ M, Sigma-Aldrich, C6628), Brefeldin A (BFA, 2 μ g/mL, Cayman Chemical, 11861), Thapsigargin (100 nM, Sigma-Aldrich, T9033), Ionomycin (100 nM, Cayman Chemical, 11932), BAPTA-AM (2 μ M, Cayman Chemical, 15551), MG-132 (10 μ M, Enzo, BML-PI102-0005), GW4869 (4 μ M, Sigma-Aldrich, D1692), Dynasore (80 μ M, Santa Cruz Biotechnology, sc-202592), Puromycin (Puro, 0.5–8 μ g/mL Invivogen, ant-pr-1), Doxycycline hyclate (Dox, 1 μ g/mL, Sigma-Aldrich, D9891).

CRISPR/Cas9 LRP10 knock-out in NPCs, HEK-293T, and HuTu-80 cells

To generate LRP10^{KO} NPCs, the Control-1 line was transfected with the pSpCas9-PuroR-LRP10gRNA plasmid using Lipofectamine™ Stem Transfection Reagent (Thermo Fisher Scientific) according to the manufacturer's specifications. The next day, 0.5 μ g/mL of Puromycin (Invivogen) was added to the NPC medium. After 2 days, scattered single cells were observed and they were allowed to recover with NPC medium without Puromycin. After 6 days, single colonies were picked and placed in 96-well plates. Recovered clones were expanded as independent clones and genotyped. HEK-293T and HuTu-80 LRP10^{KO} cells were generated according to Grochowska et al. [11, 44]. Briefly, HEK-293T and HuTu-80 cells were transfected with the pSpCas9-GFP-LRP10gRNA plasmid using GeneJuice® reagent (Merck) according to manufacturer's specifications. After 2 days, cells were dissociated with Trypsin–EDTA (Gibco), and GFP-positive cells were sorted as single cells with the BD FACSAria™ III cell sorter. Recovered clones were expanded as independent clones and genotyped. For the three cell types, we selected biallelically targeted clonal lines carrying a homozygous, single base-pair insertion, predicted to result in a premature stop codon in *LRP10* (p.Gly12Trp fs*18).

Protein lysates and conditioned media extraction

Cultured cells and brain organoids were washed with PBS and lysed with protein lysis buffer (100 mM NaCl, 1.0% Nonidet P-40 Substitute [Sigma, 74385], 50 mM Tris–Cl, pH 7.4) supplemented with protease inhibitors Complete® (Merck) and Pefabloc® SC (Merck) at 4 °C. For brain organoids, additional mechanical lysis was performed with the Disruptor Genie® (Scientific Industries, Inc.). Lysates were snap-frozen, thawed on ice, and cleared by centrifugation at 10,000 \times g for 10 min at 4 °C.

Conditioned media from cultured cells were collected, centrifuged at 10,000 \times g for 10 min at 4 °C, and further processed. When specified, cleared conditioned media was concentrated via Amicon Ultra-15 filters (Millipore, UFC901024) and centrifugation for 10–40 min at 4000 \times g at 18 °C. Each filter was used once or twice.

Western blotting

Protein lysates were mixed with 4 \times sample buffer (8% SDS, 20% v/v glycerol, 0.002% bromophenol blue, 62.5 mM Tris–Cl, pH 6.8) supplemented with 400 mM dithiothreitol (DTT) and incubated for 10 min at 95 °C. Conditioned media or EVs fractions were mixed and incubated with 4 \times sample buffer without DTT. Proteins were separated on 4–15% Criterion TGX precast gels (Bio-Rad). For experiments including control-3 and patient clone-3 brain organoids, 4–15% Stain-free Criterion TGX precast gels (Bio-Rad) were used, and they were scanned using a Gel Doc XR + Imaging System (Bio-Rad), to quantify total protein per sample. All gels were transferred to nitrocellulose membranes using the Trans-Blot® Turbo™ Transfer System (Bio-Rad). Blots that were used to detect extracellular α -synuclein were incubated with 0.4% PFA in PBS for 20 min at room temperature [52]. All membranes were blocked using 5% non-fat dry milk (Blotto, Santa Cruz Biotechnology) in Tris-buffered saline (TBS), 0.1% v/v TWEEN® 20 (Merck) for 30 min to 1 h at room temperature. Primary antibody incubations were performed in blocking buffer overnight at 4 °C. After washing in TBS, 0.1% v/v TWEEN® 20, blots were incubated for 1 h at room temperature with fluorescently conjugated secondary antibodies. After washing in TBS, 0.1% v/v TWEEN® 20, membranes were imaged and analysed using the Odyssey CLx Imaging system (LI-COR Biosciences).

Co-immunoprecipitation

After protein lysates were collected, protein concentrations were determined via Pierce™ BCA Protein Assay Kit (Thermo Fisher Scientific). For co-immunoprecipitation, Pierce™ Protein G Magnetic Beads (20 μ L, Thermo Fisher Scientific) were washed three times with washing buffer (50 mM Tris–Cl (pH 7.4), 0.5 M NaCl, 0.05% v/v TWEEN® 20) and incubated with 2 μ g of rabbit anti-LRP10 (Sino Biological, 13228-T16) or 5 μ g sheep anti-LRP10 (MRC PPU, DA058) antibody for 10 min at RT. Beads were washed three times with washing buffer and incubated with 400 μ g protein lysates overnight at 4 °C. For media fractions, 60 μ L of EVs or 1 mL of 10 \times concentrated supernatant with Amicon filters were used. Beads were washed three times with cold washing buffer and eluted with 30 μ L of 1 \times sample buffer (2% SDS, 5% v/v glycerol, 0.0005% bromophenol blue,

15.6 mM Tris–Cl (pH 6.8)) supplemented with 100 mM dithiothreitol (DTT) for 10 min at 95 °C. Beads were magnetised and discarded. Samples were analysed by western blotting.

Immunocytochemistry of 2D cultures (ICC)

Cells grown on glass coverslips were fixed with 4% PFA for 10 min and washed three times with PBS at room temperature. For uptake experiments in HuTu-80 cells, three additional washings prior to PFA incubation were performed. After washing, cells were incubated in blocking buffer (50 mM Tris.HCl, 0.9% NaCl, 0.25% gelatin, 0.2% Triton™ X-100, pH 7.4) containing primary antibodies at 4 °C overnight. Next, coverslips were washed by dipping them in a PBS, 0.05% TWEEN® 20 solution at room temperature. Cells were then incubated for 1 h with fluorescently conjugated secondary antibodies at room temperature. After washing with PBS, 0.05% TWEEN® 20, cells were mounted with ProLong Gold with DAPI (Invitrogen). For stainings with the cell surface markers AQP4, CD44, and GLAST-1, the blocking buffer consisted of PBS with 2% bovine serum albumin (BSA) and washings were performed with PBS.

Brain organoids immunocytochemistry

Brain organoids were collected in tubes, fixed with 4% paraformaldehyde (PFA, Sigma-Aldrich) for 20 min at room temperature, and washed three times with PBS. Next, they were incubated in 30% sucrose in PB buffer (23 mM NaH₂PO₄(H₂O) and 145 mM Na₂HPO₄(2H₂O) in water) at 4 °C overnight. Subsequently, they were embedded in a solution containing 7.5% gelatin and 10% sucrose in PB at room temperature. Solidified gelatin blocks were snap-frozen in cold isopentane and kept at –80 °C. Frozen gelatin blocks were cut into 20 μ m sections using a cryostat. For immunocytochemistry, sections were permeabilised and blocked with 0.25% Triton™ X-100 (Sigma-Aldrich), and 4% normal goat serum (Dako) in PBS for 1 h at room temperature. Next, they were incubated with primary antibodies diluted in 0.1% Triton™ X-100, and 4% normal goat serum in PBS at room temperature overnight. The sections were washed three times with PBS and incubated with secondary antibodies diluted in 0.1% Triton™ X-100, and 4% normal goat serum in PBS. After washing three times with PBS, the sections were mounted using ProLong Gold with DAPI (Invitrogen) and imaged on the Leica Stellaris 5 LIA confocal microscope.

Primary and secondary antibodies

The primary antibodies used for western blot (WB) and immunocytochemistry (ICC) are listed in Table 2.

Secondary antibodies used for western blot: Alexa Fluor Plus 680 or 800 donkey anti-mouse and donkey anti-rabbit (all from Thermo Fisher Scientific/Fisher, 1:1000), or Alexa Fluor® 790 AffiniPure donkey anti-sheep (Jackson immunoresearch, 1:1000).

Secondary antibodies used for immunocytochemistry: Alexa Fluor® Plus 488 donkey anti-rabbit (Thermo Fisher Scientific/Fisher), Alexa Fluor® 488 anti-mouse/sheep/goat; Alexa Fluor® 594 donkey anti-mouse, Alexa Fluor® 647 goat anti-guinea pig (Jackson ImmunoResearch Laboratories).

Antibodies used for TEM: goat anti-rabbit IgG 15 nm gold-labelled (Aurion, 815.011), ImmunoGold goat anti-mouse 6 nm gold-labelled (Aurion, 806.022).

Microscopy images acquisition

Brain organoids and protein uptake specimens were imaged with the Leica Stellaris 5 LIA confocal microscope. The following lasers were used: diode 405, OPSL 488, DPSS 561, and diode 638. Each image was detected with the 3 \times spectral HyD S detector with an HC PL APO CS2 40 \times /1.3 or HC PL APO CS2 63 \times /1.4 lens. The rest of the specimens were imaged with Leica SP5 AOBS confocal microscope. The following lasers were used: diode 405, OPSL 488, DPSS 561, and HeNe 633. Each image was detected on the spectral PMT detector with an HCX PL APO CS 40 \times /1.25 or HCX PL APO CS 63 \times /1.4 lens. For both microscopes, scanning of detailed images was done with a pixel size of 0.1 μ m and with a scan size of 2048 \times 2048 pixels at 400 or 600 Hz. For z-stack images, 0.35 μ m steps in the z-direction were taken. The pinhole size was set to 1 airy unit (AU). Scanning of overview brain organoids images consisted of a tile scan of 9 regions with a pixel size of 0.285 μ m, a scan size of 1024 \times 1024 pixels at 600 Hz, and 0.5 μ m steps in the z-direction.

Image analysis

Microscopy images were analysed using Fiji/ImageJ version 1.45b. For colocalisation of LRP10 and cellular markers in control brain organoids, big artifacts and background signal were removed from each channel using automatic thresholding and size filtering. The built-in tool coloc2 was used to determine the Manders' coefficient. The channels overlap of each Z plane was averaged for each brain organoid. The rest of analyses were performed on maximum projections. To quantify LRP10 uptake in HuTu cells, a mask for cell surfaces was generated using the LRP10 antibody channel including background signal from the cell cytoplasm. LRP10 signal was then measured from individual cells after automatic thresholding and generating a mask exclusively containing overlapping signal from the LRP10 antibody and

Table 2 Primary antibodies used for immunocytochemistry (ICC) and western blotting (WB) experiments

Target protein	Host	Supplier	Catalogue number	WB dilution	ICC dilution
AQP4	Rabbit	Sigma-Aldrich	HPA014784	–	1:100
APC	Mouse	Abcam	AB16794	–	1:100
calnexin	Rabbit	Cell Signaling Technologies	2679S	1:2000	–
CD44	Mouse	Abcam	ab6124	–	1:100
CD63	Mouse	ThermoFisher	10628D	1:1000	–
CD81	Mouse	ThermoFisher	10630D	1:1000	–
EEA1	Mouse	BD Biosciences	610,457	–	1:200
FOXA2	Rabbit	Cell Signaling Technologies	8186	1:1000	–
GFAP	Mouse	DSHB	N206A/8	–	1:200
GFAP	Rabbit	Sigma-Aldrich	AB5804	1:1000	1:200
GLAST-1	Rabbit	Novus	NB100-1869SS	–	1:100
LRP10* (N-t)	Rabbit	Sino Biological	13,228-T16	1:1000	1:200
LRP10 (C-t)	Sheep	MRC PPU	DA058	1:1000	–
MAP2	Guinea pig	Synaptic systems	188 004	–	1:500
NANOG	Rabbit	Abcam	AB21624	–	1:75
OCT4	Rabbit	Abcam	AB19857	–	1:250
SOX9	Goat	R&D Systems	AF3075-SP	–	1:100
SSEA4	Mouse	Abcam	AB16287	–	1:75
s100 β	Mouse	Sigma-Aldrich	S2532	–	1:200
TGN46	Sheep	Bio-Rad	AHP500GT	–	1:300
TH	Sheep	Novus	NB300-110	1:1000	–
TRA1-81	Mouse	Abcam	AB16289	–	1:75
tubulin β 3	Mouse	Abcam	AB78078	1:5000	–
vinculin	Mouse	Santa Cruz Biotechnology	2679S	1:5000	–
α -synuclein	Mouse	BD Biosciences	610,787	1:1000	–

“*” = This antibody, raised against the N-terminal domain of LRP10, was used for LRP10 detection in all experiments unless otherwise specified

mCherry channels. To quantify LRP10 in neurons in DMSO and BafA1-treated brain organoids, 30 MAP2-positive neurons were randomly selected from two brain organoids per condition, and their cell surface was manually outlined after generating short maximum projections (3–5 planes of 0.5 μ m each) that were adjusted per cell. LRP10 signal intensity was measured from each cell. To study LRP10 levels in s100 β -positive cells in control and patient brain organoids, a mask for s100 β was generated after automatic thresholding. LRP10 objects within the s100 β mask were measured after an additional automatic thresholding step. To quantify the mean intensity and area % of LRP10 wild-type (LRP10^{WT}) and the patient-derived LRP10 splice variant (LRP10^{splice}) in overexpressing cells, the cell surfaces of single cells were selected using the LRP10 antibody channel including background signal from the cell cytoplasm, and LRP10 signal was quantified per cell after automatic thresholding.

EVs isolation from conditioned media

HEK-293T cells were grown in T75 cell culture flasks and refreshed 2 days before media collection with exosome-free

growth media (FBS was replaced by One Shot™ Fetal Bovine Serum, Exosome-Depleted, Gibco) supplemented with GW4869 or DMSO when indicated. Ten millilitres of conditioned media were collected and centrifuged at 2000 \times g for 10 min at 18 °C to remove cell debris. The initial supernatant (also referred to as “whole media”) was collected and further centrifuged at 16,000 \times g for 20 min at 4 °C to remove big vesicles. The resulting supernatant was filtered with a membrane pore size of 0.2 μ m (Whatman) and centrifuged at 120,000 \times g for 4 h at 4 °C in polycarbonate bottle assemblies (Beckman coulter, 355,603) in a 70.1 Ti fixed angle rotor (Beckman coulter, 342184) in an Optima XE-90 ultracentrifuge (Beckman coulter) to collect smaller EVs, including exosomes. The final supernatant was collected as the “supernatant” fraction and the pellet was resuspended with 70 μ L of PBS (“Evs” fraction). Evs were further processed or stored at –80 °C.

iPSC-derived astrocytes were grown in T25 flasks with exosome-free N2 medium (FBS was replaced by One Shot™ Fetal Bovine Serum, Exosome-Depleted, Gibco), and conditioned media was collected and frozen at –80 °C four consecutive times with a 2-day interval. Twenty

millilitres of media were then thawed on ice, centrifuged at $2000\times g$ for 10 min at 18 °C, and the supernatant was concentrated until reaching a volume of 10 mL with Amicon filters. The concentrate was collected and further centrifuged at $16,000\times g$ for 20 min at 4 °C, filtered with a 0.2 μm membrane, and ultracentrifuged at $120,000\times g$ for 4 h at 4 °C. The final supernatant was collected (“supernatant” fraction) and the pellet (“EVs fraction”) was resuspended with 70 μL of PBS.

EV quantification (EVQuant)

EVs were quantified using the recently developed EVQuant assay, described previously [53]. Briefly, isolated EVs, supernatant, and whole media fractions were mixed with the fluorescent membrane dye Octadecyl Rhodamine B Chloride R18 (0.33 ng/ μL , Life Technologies, O246) and incubated for 10 min at room temperature. Next, fluorescently labelled EVs were immobilised in a non-denaturing polyacrylamide gel (16% w/w acrylamide/bis-acrylamide) in 96-well glass-bottomed plates (Cellvis, P96-0-N). Per sample, 25 single-plane images were acquired using a high-content screening system (Opera Phenix, Perkin Elmer) using a $40\times$ water immersion objective (NA 1.1). Rhodamine-labelled nanoparticles were excited using a 561nm laser and detected at 570–630 nm emission wavelength. EV concentration was calculated as the number of detected EVs in a calibrated confocal imaging volume [53]. EV concentrations were background corrected using a dye-only control (sample containing PBS mixed with Rhodamine).

Transmission electron microscopy (TEM)

EVs purified from conditioned media were evaluated by TEM. To prepare samples for TEM, 10 μL of isolated EVs were incubated for 20 min with a formvar/carbon-coated 400 mesh copper grid. Next, the grids were washed 3 times with PBS, incubated for 30 min with 10 μL of blocking solution containing normal goat serum (Aurion, 905.002), and washed two times with 0.1% BSA-c (Aurion, 900.099). Primary antibodies (rabbit anti-LRP10, mouse anti-CD81, or mouse anti-CD63, 1:50) were diluted in 0.1% BSA-c and added to the samples for 1 h. The grids were washed four times with 0.1% BSA-c and incubated for 1 h with the gold-coupled secondary antibodies diluted in 0.1% BSA-c (1:50 dilution). Next, they were washed five times with 0.1% BSA-c, three times with PBS, and three times with ultrapure water. Grid staining was performed with Uranylless EM Stain for 1 min (negative stain). Grids were air-dried and

visualised with a TALOS L120C TEM at 120kV at 11–45 k magnification.

Nanoparticle tracking analysis (NTA)

NTA was used to quantify and characterise isolated EVs from iPSC-derived astrocytes or exosome-free astrocyte media (Advanced DMEM/F-12, 4% exosome-free FBS, 1% N2, 1% Penicillin–Streptomycin), and HEK-293T cells or exosome-free HEK-293T media (DMEM, 10% exosome-free FBS, 1% Penicillin–Streptomycin) with the NanoSight NS3000 system (Malvern, Sysmex) in light scatter mode using the 405 nm laser. Samples were diluted 1:10 in DPBS (Gibco) and three consecutive measurements were performed for 60 s at a controlled temperature of 25 °C.

Conditioned media uptake

HEK-293 cells were cultured in growth medium in 10 cm cell culture dishes. The day before media collection, cells were refreshed with DMEM. Next, 10 mL of conditioned media was collected and centrifuged at $2000\times g$ for 10 min. The supernatant was concentrated $100\times$ with Amicon concentrating filters and mixed with fresh media until reaching a final concentration of $10\times$. For uptake of LRP10 in HuTu-80 cells, cells were washed with PBS and refreshed with DMEM:F12 (Gibco, 11320–074) supplemented with DMSO or 80 μM Dynasore for 30 min, prior to the addition of 1:10 conditioned media concentrate for 30 additional min before further processing. For additional uptake experiments, 1:10 conditioned media concentrate was mixed with growth medium and placed on the donor cells for the specified time points.

Statistical analysis

Statistical analyses were performed using Prism 9 software (GraphPad). For experiments with only two conditions, Student’s *t*-test or Mann–Whitney test were used. For experiments with two or more groups, one-way or two-way ANOVA followed by the Dunnett’s, Tukey’s, or Sidak’s multiple comparisons tests were used. The Grubb’s test was used to discard outliers. Significant *P* values of $P \leq 0.05$ were reported. In the graphs, “*” represents a *P*-value of $P \leq 0.05$, “**” represents $P \leq 0.01$, “***” represents $P \leq 0.001$, and “****” represents $P \leq 0.0001$. The data are presented as means \pm standard deviations (SD) and represent results from at least two biological replicates.

Results

LRP10 is secreted via extracellular vesicles and is sensitive to autophagic function

Work from Grochowska et al. [11] revealed that LRP10 is mainly expressed in non-neuronal cells in adult human brain. However, in LBD cases, LRP10 was also detected in Lewy bodies within dopaminergic neurons. To address whether LRP10 in neuronal Lewy bodies possibly originates from non-neuronal cells, we first investigated LRP10 secretion in cultured cells. We studied LRP10 distribution in cell lysates and conditioned media from LRP10-overexpressing (OE) HEK-293T cells by western blot analyses. As a result, LRP10 was detected in both fractions 48 h after transfection (Fig. 1A). LRP10 is a transmembrane protein, so we hypothesised that LRP10 would partition to a lipid membrane-containing fraction, potentially EVs. To address this issue, we fractionated conditioned media (referred to as “whole media”) via sequential centrifugation, filtration, and ultracentrifugation, which resulted in a pellet—consisting of small EVs [54]—and supernatant fractions (Supplementary Fig. 1A). Effectiveness of the isolation was demonstrated via different methods [54]. First, western blot analyses revealed the presence of the EVs markers CD63 and CD81 and the absence of the ER-resident protein calnexin in the whole media and EVs fractions (Supplementary Fig. 1B). The absence of calnexin in media fractions also indicated the lack of cell death-related contamination. Next, particle count quantification via membrane-labelling via EVQuant [53] demonstrated the successful concentration of EVs from whole media (Supplementary Fig. 1C; LRP10 wild-type (LRP10^{WT}) whole media mean: 4×10^{10} particles; supernatant mean: 9×10^9 particles; EVs mean: 4×10^{11} particles). Finally, nanoparticle tracking analysis (NTA) was used to determine the size of the purified EVs, which presented a mean diameter of $135.5 \text{ nm} \pm 69.7$ and a mode of 84.5 nm (Supplementary Fig. 1D), which is in line with the expected size of exosomes (50–150 nm) and other EVs subtypes [54]. Furthermore, NTA also showed an enrichment of vesicles after EVs purification from conditioned media in comparison to media that had not been in contact with cells (Supplementary Fig. 1D). To prove that LRP10 is secreted via EVs, we used LRP10-overexpressing cells and treated them with DMSO or GW4869, a compound that inhibits exosome release. After 2 days, protein extracts and conditioned media were collected, and EVs were isolated. LRP10 was found in the EVs fraction (Fig. 1B and Supplementary Fig. 1B) but not in the supernatant fraction (Supplementary Fig. 1B). Furthermore, LRP10 levels in EVs were significantly lower after GW4869 treatment

with a sixfold reduction (Fig. 1C). To further confirm the presence of LRP10 in EVs, we performed immuno-transmission electron microscopy (TEM) and labelled LRP10, CD63, and CD81 with golden particles in isolated EVs from conditioned media (Fig. 1D). This assay also confirmed the successful isolation of vesicular structures of the expected sizes (diameter of 50–150 nm for exosomes) [54]. Taking these observations together, we conclude that LRP10 is secreted via EVs.

To gain more mechanistic insight into LRP10 secretion, we treated control and LRP10-overexpressing HEK-293T cells for 4 h with compounds that alter cellular functions involved in different secretion pathways and studied their effect on the intra- and extracellular distribution of LRP10 via western blot (Fig. 1E). Brefeldin A (BFA), an ER-to-Golgi vesicle transport and conventional secretion inhibitor, induced a significant increase in intracellular levels of LRP10, but did not affect extracellular LRP10 levels, suggesting that LRP10 follows an unconventional secretory pathway (Fig. 1E–G). Thapsigargin, an ER stressor that blocks Ca^{2+} entry into the ER, did not change the amount of intracellular LRP10 but decreased LRP10 extracellular levels. BafA1, a vacuolar H^+ ATPase inhibitor that blocks vesicle acidification and autophagy, increased LRP10 intracellular levels and induced a striking sevenfold increase in LRP10 secretion (Fig. 1E–G). Additionally, BafA1 treatment also led to the detection of endogenous LRP10 in conditioned media from control cells. Torin1, which promotes autophagic function, led to a decrease in intracellular LRP10 without affecting extracellular LRP10 levels. Methylamine and chloroquine (CQ), which inhibit vesicle acidification by different mechanisms, had no effect on intra- and extracellular LRP10 levels, nor did the Ca^{2+} level modifiers BAPTA-AM and Ionomycin (Fig. 1E–G). Taken together, these results show that LRP10 is secreted via EVs, and can be significantly enhanced after blockade of the autophagy pathway.

Due to their relatively high LRP10 expression levels [11, 55–57], we used a previously established in vitro iPSC-derived astrocytes model [11, 49] to study the effect of BafA1 treatment on LRP10 under more physiological conditions. Successful generation of control astrocytes derived from a control donor and knock-out (LRP10^{KO}) astrocytes was confirmed via immunocytochemistry for the astrocytic markers glial fibrillary acidic protein (GFAP), S100 calcium-binding protein β (s100 β), SRY-box transcription factor 9 (SOX9), aquaporin 4 (AQP4), CD44, and Glutamate/Aspartate transporter 1 (GLAST-1) (Supplementary Fig. 2). To determine whether autophagic inhibition affects endogenous LRP10 intracellular levels, control astrocytes were treated with BafA1 for 4 h, and cell lysates were analysed via western blotting (Fig. 1H). As a result, we observed a two-fold increase of LRP10

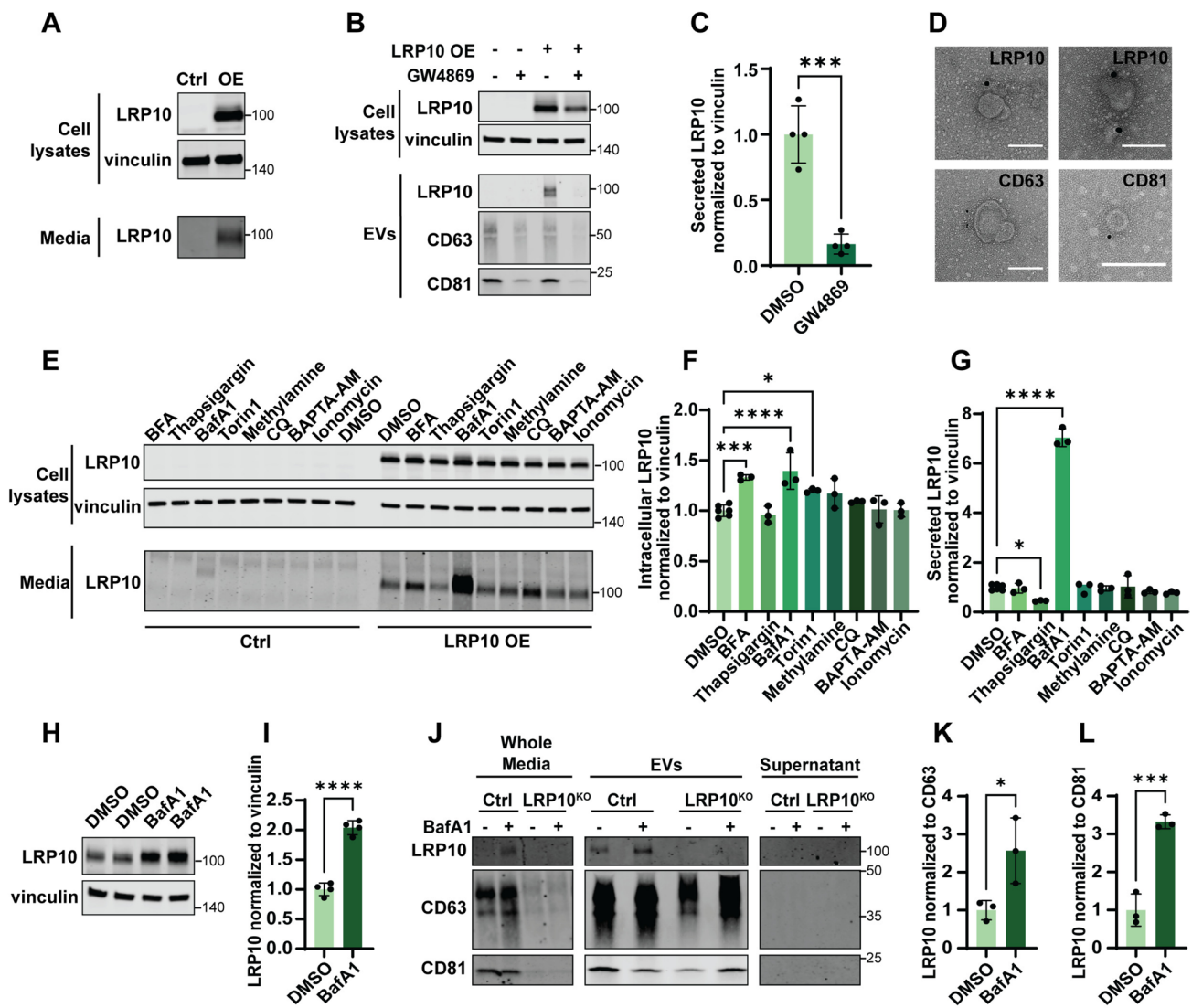


Fig. 1 LRP10 secretion mechanisms. **A** Representative western blot of cell lysates and conditioned media from control (Ctrl) and LRP10-overexpressing (OE) HEK-293T cells probed for LRP10 and vinculin. **B** Representative western blot of cell lysates and EVs isolated from conditioned media from LRP10-overexpressing cells after 48 h of DMSO or GW4869 treatments. Blots were probed for expression of LRP10, vinculin, CD63, and CD81. **C** Western blot quantification of LRP10 in EVs normalised to vinculin in cell lysates from **B**. *N*=4 biological replicates. **D** Representative TEM images of LRP10, CD63, and CD81 immunoreactive EVs. Scale bars=100 nm. **E** Representative western blot of LRP10-overexpressing cells treated with the indicated compounds for 4 h. **F, G** Western blot quantifications of intracellular (**F**) and extracellular (**G**) LRP10 normalised to intracellular vinculin from **E**. *N*=3 biological replicates. **H, I** Rep-

resentative western blot (**H**) and quantification (**I**) of endogenous LRP10 in 2-month-old control iPSC-derived astrocytes treated with DMSO or BafA1 for 4 h. *N*=4 biological replicates. **J** Representative western blot of fractionated conditioned media from 4-month-old control and LRP10^{KO} iPSC-derived astrocytes after 2 days in culture with exosome-free media followed by a 6 h treatment with DMSO or BafA1. Conditioned media (Whole Media) was fractionated into EVs and supernatant fractions. **K, L** Quantification of LRP10 in EVs normalised to the EVs markers CD63 (**K**) and CD81 (**L**) from (**J**). *N*=3 biological replicates. All data are expressed as mean \pm SD with individual data points shown. Data in **C, I, K, L** were analysed by unpaired *T*-test. Data in **F, G** were analysed by One-way ANOVA with Dunnett's multiple comparisons test. **P* \leq 0.05, ****P* \leq 0.001, *****P* \leq 0.0001

intracellular levels after BafA1 treatment (Fig. 1I). Next, to study LRP10 secretion, control and LRP10^{KO} astrocytes were cultured for 2 days in exosome-free media and treated with DMSO or BafA1 6 h before conditioned media was collected and fractionated. Western blot analyses revealed the presence of LRP10 in EVs from control astrocytes, but

not in the supernatant fraction (Fig. 1J). Furthermore, we observed a significant 2.6- to 3.3-fold increase in LRP10 in EVs in BafA1-treated control astrocytes (Fig. 1K and L). Strikingly, LRP10 was already detected in whole media from BafA1-treated control astrocytes (Fig. 1J). In addition to presenting CD63 and CD81 (Fig. 1J), the purified EVs

were also characterised via NTA (Supplementary Fig. 1E), which showed a peak in the EVs diameter of 140.5 nm. To conclude, autophagic inhibition induces an increase in LRP10 intracellular levels and secretion, particularly via EVs, in iPSC-derived astrocytes, which is in line with our observations using LRP10-overexpressing cells (Fig. 1E–G).

LRP10 is internalised via clathrin-mediated endocytosis

We next investigated whether secreted LRP10 can be internalized by acceptor cells. We used mCherry-LRP10-overexpressing HEK-293T cells to produce and secrete mCherry-LRP10 into conditioned media, and after 48 h we placed it onto Dynasore (clathrin-mediated endocytosis inhibitor) [58]-treated LRP10^{KO} cells for 30 min. Recipient cells were subsequently inspected via immunocytochemistry for the presence of double-positive vesicles containing both mCherry signal and signal from our KO-validated LRP10 antibody to increase specificity (Fig. 2A) [11]. We observed several double-positive vesicles that were also colocalising with the endosomal marker early endosome antigen 1 (EEA1) (Fig. 2A). Additionally, a significantly lower number of double-positive vesicles were detected after Dynasore

treatment (Fig. 2B), which also presented lower LRP10 signal intensity (Fig. 2C). These findings suggest that LRP10 can be internalised via clathrin-mediated endocytosis.

LRP10 expression is enriched in astrocytes in brain organoids

To address whether the origin of LRP10 in Lewy bodies could be the result of an interaction between different brain cell types, we turned to brain organoids as a model system. Control iPSCs were differentiated into brain organoids according to published protocols [50, 51]. Even though these brain organoids are described to be partially functional after 1 month in vitro, astrocyte markers start appearing after 2 months in culture [51]. This observation is in line with normal neurodevelopment, where astrocytes are specified later than neurons [59]. Therefore, we characterised our brain organoids at 2 and 4 months after the start of differentiation by immunocytochemistry and western blotting analyses (Supplementary Fig. 3). We detected various cell types, including neurons (Supplementary Fig. 3A), astrocytes (Supplementary Fig. 3B), and oligodendrocytes (Supplementary Fig. 3C), in addition to the presence of tyrosine hydroxylase (TH) and forkhead box protein A2 (FOXA2),

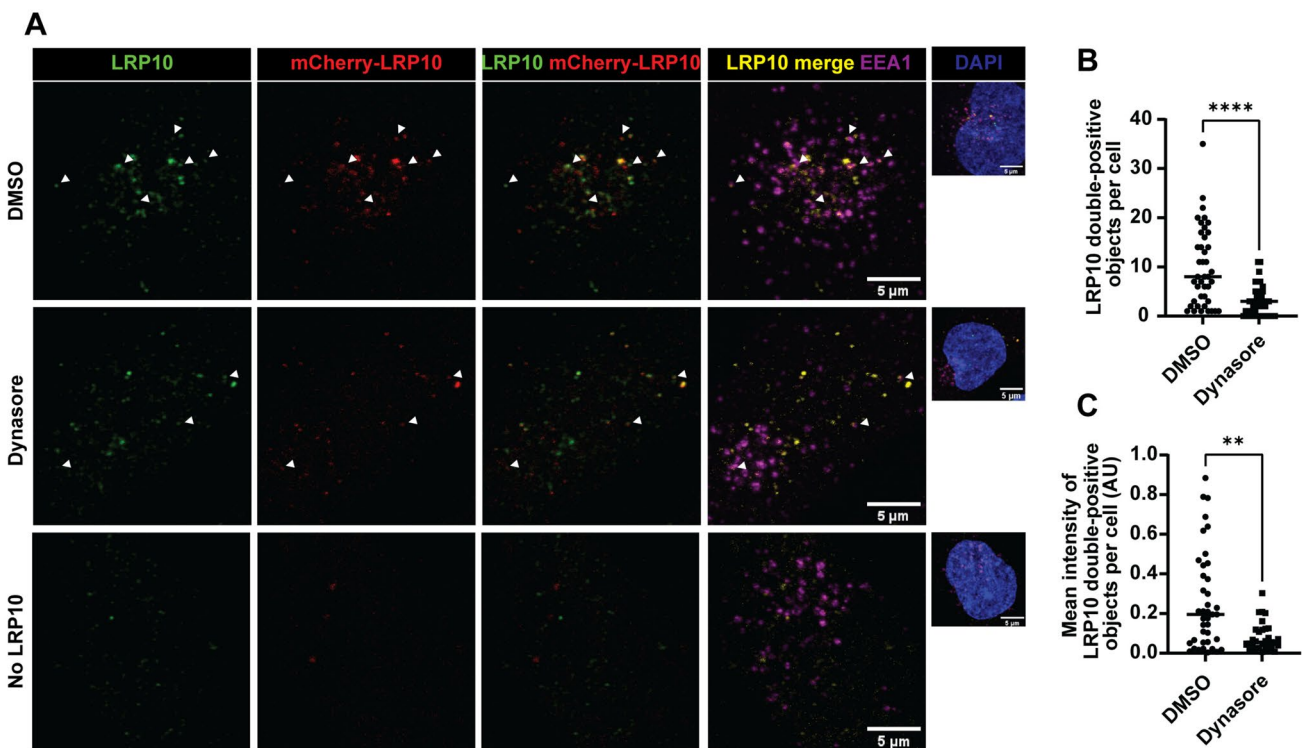


Fig. 2 LRP10 uptake via clathrin-mediated endocytosis. **A** Representative confocal images of LRP10 and mCherry-LRP10 internalised by DMSO or Dynasore-treated LRP10^{KO} HuTu-80 cells. White arrowheads indicate LRP10 in EEA1-positive vesicles. **B**, **C** Quantifications of LRP10 double-positive objects (**B**) and their sig-

nal intensity (**C**) per cell. $N \geq 40$ biological replicates. All data are expressed as mean \pm SD with individual data points shown. Data were analysed by Mann–Whitney test. ** $p = 0.0014$ ($p < 0.01$), **** $P \leq 0.0001$

a developmental midbrain-specific marker [60] (Supplementary Fig. 3D and E). From 2 to 4 months in culture, we observed increased levels of several markers, including LRP10 (1.7-fold, not significant), FOXA2 (fourfold, not significant), and the astrocytic marker GFAP (18-fold, $**P = 0.0026$). Therefore, 4-month-old brain organoids were selected for further testing due to their higher astroglial levels.

To investigate LRP10 cellular localisation and test whether the findings on LRP10 restricted cell-type expression pattern in human brain material could be reproduced in brain organoids, we performed immunocytochemistry and subsequent colocalisation analysis between LRP10 and different cellular markers in control brain organoids (Fig. 3A and B). As a result, LRP10 showed a 20% overlap with the neuronal marker microtubule-associated protein 2 (MAP2), a 61% overlap with the astrocytic marker s100 β , and a 3% overlap with the oligodendrocytic marker Quaking 7 (QKI-7) [61] (Fig. 3B). Therefore, LRP10 localisation in brain organoids is enriched in astrocytes, which is in line with previous findings in human post-mortem brain material [11].

Autophagy inhibition induces the formation of atypical LRP10 objects in neurons of brain organoids

Accumulating evidence suggests that defective autophagic function might play an important role in PD and DLB pathogenesis [62]. Since we show that inhibition of the autophagy pathway via BafA1 treatment leads to increased LRP10 secretion, we speculate that defective autophagy in LBD brains could be a potential cause for enhanced LRP10 secretion from non-neuronal cells and subsequent neuronal uptake and accumulation in Lewy bodies. To investigate this possibility, we treated control brain organoids with DMSO or BafA1 for 4 h and studied LRP10 levels and localisation via immunocytochemistry (Fig. 3C–H). First, we observed 1.7-fold higher LRP10 levels in whole brain organoids after BafA1 treatment (Fig. 3C and D), which is in line with the observed effect of BafA1 on LRP10-overexpressing cells and astrocytes (Fig. 1E–I). Inspection of LRP10 localisation relative to the astrocytic marker s100 β and the neuronal marker MAP2, revealed that LRP10 remained enriched in astrocytes in comparison to neurons before and after BafA1 treatment (Fig. 3C, E, and H). However, analysis of single MAP2-positive neurons showed a significant twofold increase in LRP10 signal after BafA1 treatment, as well as neurons with atypical enlarged LRP10+ intracellular vesicular structures (Fig. 3F and G). To exclude the possibility of BafA1-induced cell death, we performed a lactate dehydrogenase (LDH) toxicity assay in HEK-293T cells treated for 6 h, which showed no difference in fraction of dead cells in 200 nM BafA1 and DMSO-treated cells (Supplementary Fig. 4A). Furthermore,

quantification of signal intensity of cellular markers (DAPI, s100 β , and MAP2) in the studied organoids (Fig. 3) did not show evidence of increased cell death upon 4 h BafA1 treatment (Supplementary Fig. 4B). These data show that autophagic stress induces an increase in LRP10 levels in brain organoids in astrocytes and neurons, and the formation of atypical LRP10 vesicular structures in neurons.

LRP10 overexpression affects α -synuclein intracellular levels and secretion

The aggregation and associated neuronal toxicity of α -synuclein are considered to be central in PD and DLB pathogenesis. Since both LRP10 and α -synuclein are found in Lewy bodies [11], we sought to study a possible functional link between LRP10 and α -synuclein. First, we overexpressed variable amounts of both proteins (encoded by *LRP10* and *SNCA*, respectively) in HEK-293T cells to investigate their interaction after two days via western blot (Fig. 4A). Interestingly, α -synuclein overexpression led to a significant decrease in intracellular LRP10 levels (Fig. 4B), and, in contrast, LRP10 overexpression induced increased intracellular α -synuclein levels (Fig. 4C). The strongest effect was found in the media fraction, where we observed a striking 150 to 300-fold increase in extracellular α -synuclein levels in the condition of combined α -synuclein and LRP10 overexpression (Fig. 4D). These results indicate that LRP10 and α -synuclein have an opposite, reciprocal effect on the intracellular levels of the other protein, and that LRP10 promotes α -synuclein secretion.

To better understand the dynamics of the LRP10– α -synuclein interaction, we examined the effect of LRP10 overexpression on intra- and extracellular α -synuclein levels over time using the same experimental paradigm (Fig. 4E). LRP10 overexpression led to elevated intracellular α -synuclein levels at 48 h post-transfection when compared to control cells, but this initial effect was reversed from 72 h onwards (Fig. 4F). In the media fraction, control cells showed a slight increase in α -synuclein levels from 96 h onwards, whereas LRP10-overexpressing cells showed a peak in extracellular α -synuclein levels at 48 h post-transfection (Fig. 4G). Nonetheless, LRP10-overexpressing cells showed higher extracellular α -synuclein levels than control cells overall (LRP10 OE vs Control: $****P < 0.0001$). To conclude, LRP10 dynamically modulates intracellular α -synuclein levels over time and strongly promotes its secretion.

LRP10 induces α -synuclein secretion via unconventional secretion pathways

Several studies have shown that α -synuclein is secreted via a variety of pathways, including EVs [63, 64]. To determine whether LRP10 promotes α -synuclein secretion via EVs, we purified EVs from conditioned media of LRP10

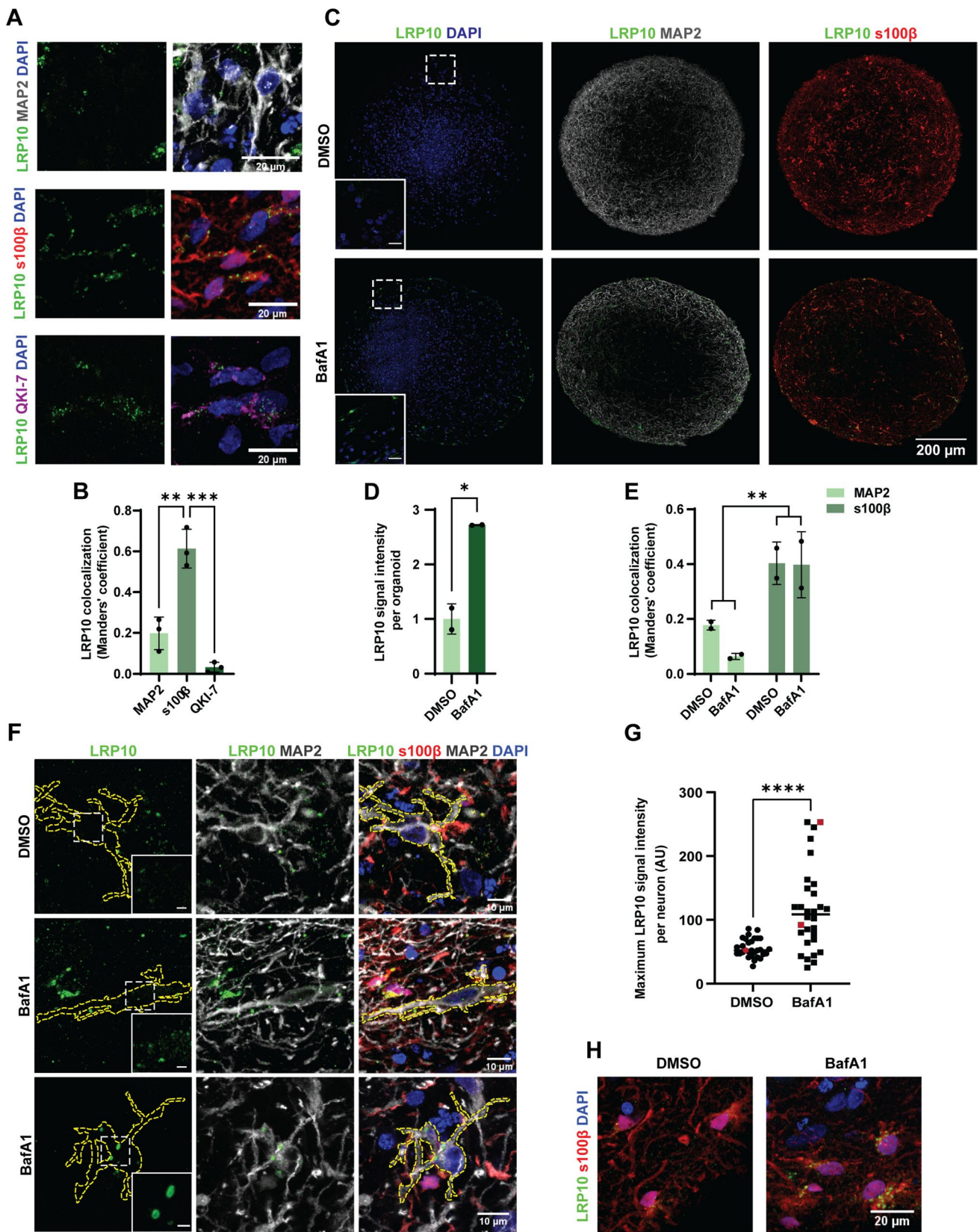


Fig. 3 LRP10 localisation in untreated and BafA1-treated brain organoids. **A** Representative confocal images of LRP10 localisation in 2-month-old control, untreated brain organoids relative to the cellular markers MAP2 (neurons), s100 β (astrocytes), and QKI-7 (oligodendrocytes). **B** Colocalisation analysis via Manders' overlap of LRP10 with MAP2, s100 β , and QKI-7 from **A**. $N=3$ biological replicates. **C** Representative tile scans of LRP10 in 4-month-old control brain organoids treated with DMSO or BafA1 for 4 h relative to the markers MAP2 and s100 β . White dotted boxes indicate the zoomed-in regions in the bottom left corners (Scale bars = 20 μ m). **D, E** Quantification of LRP10 signal intensity (**D**) and LRP10 colocalisation with MAP2 (neurons) and s100 β (astrocytes) (**E**) per brain organoid from **C**. $N=2$ biological replicates. **F** Representative detailed confocal images of LRP10 in MAP2-positive neurons in DMSO or BafA1-treated brain organoids from **C**. The cell surface of single MAP2-positive cells is indicated with yellow dotted lines. White dotted boxes indicate the zoomed-in regions for LRP10 in the bottom right corners for the LRP10 channel (Scale bars = 2 μ m). **G** Quantification of LRP10 maximum signal intensity per MAP2-positive neuron. Red data points indicate the values of the representative cells shown in **F**. $N=30$ MAP2-positive cells derived from 2 brain organoids per condition. **H** Representative detailed confocal images of LRP10 in s100 β -positive astrocytes in DMSO or BafA1-treated brain organoids from **C**. All data are expressed as mean \pm SD with individual data points shown. Data from **B** were analysed by One-way ANOVA with Tukey's multiple comparisons test. Data from **D** were analysed by unpaired T-test. Data from **E** were analysed by Two-way ANOVA. Data from **G** were analysed by Mann-Whitney test. * $P \leq 0.05$, ** $P \leq 0.01$, *** $P \leq 0.001$, **** $P \leq 0.0001$

and α -synuclein-overexpressing cells treated with DMSO or GW4869 for 48 h. Western blotting revealed the presence of α -synuclein in the EVs and the supernatant fractions (Fig. 5A). In both fractions, LRP10 overexpression induced a significant increase in α -synuclein levels (Fig. 5B). In contrast to the inhibitory effect of GW4869 treatment on LRP10 localisation in EVs, GW4869 induced an increase in α -synuclein levels in EVs, which suggests the activation of an alternative secretion pathway (Fig. 5A and B, DMSO vs GW4869 * $P=0.0305$). Additionally, GW4869 treatment did not affect α -synuclein secretion differently in LRP10-overexpressing cells in comparison to control cells (Fig. 5C). These data indicate that LRP10 induces α -synuclein secretion via EVs and EVs-independent mechanisms.

To study the involvement of other secretory pathways in LRP10-mediated α -synuclein secretion, we focused on pathways that we demonstrated to affect intra- and extracellular LRP10 levels (Fig. 1E–G). To this aim, we used LRP10 and α -synuclein-overexpressing cells and analysed α -synuclein secretion after the different treatments. BFA treatment induced a significant increase in α -synuclein secretion over time in control cells, but not in LRP10-overexpressing cells (Fig. 5D and E), suggesting that BFA treatment induces an alternative α -synuclein secretion pathway only in control cells. Next, Thapsigargin treatment induced a more significant and prolonged decrease in α -synuclein secretion in LRP10-overexpressing cells (Fig. 5F and G).

In contrast, treatment with BafA1 resulted in a decrease in α -synuclein levels in both control and LRP10-overexpressing cells (Fig. 5H and I). Finally, MG-132 treatment, which blocks the proteasome degradation pathway, significantly blocked LRP10-mediated α -synuclein secretion, with no effect on α -synuclein secretion in control cells (Fig. 5J and K). Combined, these data show that LRP10-mediated α -synuclein secretion is influenced by ER stress and proteasomal function.

LRP10-variant-carrying patient cells show defects in LRP10 expression and secretion

Work from Quadri et al. [9] identified two heterozygous *LRP10* genetic variants in genomic position *c.1424+5* in DLB and PD patients. These variants were shown to interfere with *LRP10* mRNA splicing, resulting in the appearance of a premature stop codon in the variant-carrying allele (Fig. 6A and Supplementary resource 1), which ultimately results in a shorter truncated protein lacking most functional domains and the transmembrane domain (LRP10^{splice}, Fig. 6B).

Here, we studied LRP10^{splice} in cells derived from a late-onset DLB patient carrying a heterozygous *c.1424+5G>A* variant in *LRP10* [9]. We first generated iPSC lines derived from this patient and a control individual and characterised them via immunocytochemistry and qPCR for expression of pluripotency markers (Table 1, Supplementary Fig. 5, control-3 and patient clones 1–3). Brain organoids were generated from control-3 and patient clone-3 iPSCs and were characterised via immunocytochemistry (Supplementary Fig. 6A, 4-month-old brain organoids) and western blot analyses (Supplementary Fig. 6B–F, 2 and 4-month-old brain organoids), which revealed the presence of neurons (MAP2, tubulin- β 3, and α -synuclein), astrocytes (GFAP), and oligodendrocytes (QKI-7) in both lines. Both the control-3 and the patient clone-3 lines showed a significant increase in GFAP levels from 2 to 4 months in culture (Supplementary Fig. 6F), similar to the previously characterised control-1 line (Supplementary Fig. 3E). We subsequently analysed LRP10 distribution in control and LRP10^{splice} brain organoids. Since astrocytes present high endogenous LRP10 levels [11, 55, 56], we analysed LRP10 expression in s100 β -positive astrocytes via immunocytochemistry. As a result, we found a significant reduction in LRP10 signal intensity within s100 β -positive astrocytes in patient brain organoids when compared to controls (Fig. 6C and D). However, western blot analyses revealed that the total amount of LRP10 in brain organoids was not significantly different between the two brain organoid lines (Supplementary Fig. 6B and C). Therefore, LRP10^{splice} brain organoids produce relevant

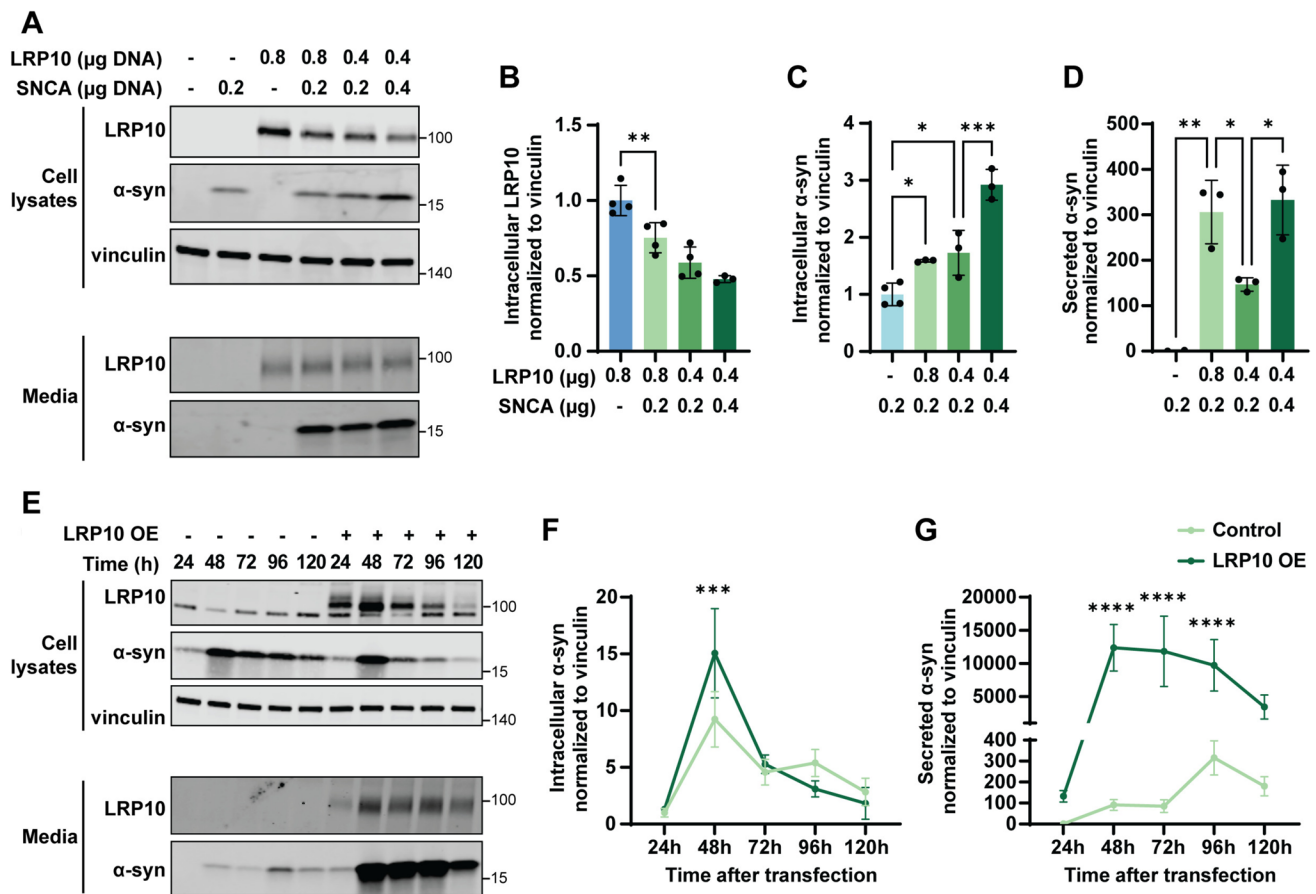


Fig. 4 LRP10 and α -synuclein interaction. **A** Representative western blot of cell lysates and conditioned media from HEK-293T cells transfected for 48 h with different amounts of *LRP10* and *SNCA*. **B–D** Western blot quantifications of intracellular LRP10 (**B**), intracellular α -synuclein (α -syn) (**C**), and secreted α -synuclein normalised to intracellular vinculin (**D**). $N=4$ biological replicates. **E** Representative western blot of cell lysates and conditioned media from

LRP10 and α -synuclein-overexpressing cells over time. **F**, **G** Western blot quantifications of intracellular α -synuclein (**F**) and secreted α -synuclein (**G**) normalised to intracellular vinculin. $N=3$ biological replicates. All data are expressed as mean \pm SD with individual data points shown in **B–D**. Data in **B–D**, **F**, **G** were analysed by One-way ANOVA with Sidak's multiple comparisons test. * $P \leq 0.05$, ** $P \leq 0.01$, *** $P \leq 0.001$, **** $P \leq 0.0001$

neural cell types and present an altered LRP10 signal distribution in s100 β -positive astrocytes.

To further investigate the patient-derived LRP10 species, two iPSC clones from the LRP10^{splice} variant-carrying patient (clones 1 and 2: P1 and P2) and two control lines (controls-1 and -2: C1 and C2) iPSC lines were differentiated into astrocytes according to published protocols [11, 49]. Patient iPSCs were characterised via immunocytochemistry and qPCR for expression of pluripotency markers (Supplementary Fig. 5, patient clones 1 and 2). To determine the efficiency of the differentiation protocol, astrocyte cultures were characterised at 2 months after the start of the differentiation via immunocytochemistry, which showed expression of the astrocytic markers GFAP, SOX9, AQP4, and s100 β (Supplementary Fig. 7). After 4 months of differentiation, LRP10 intra- and extracellular distribution was investigated in astrocyte cell lysates and fractionated conditioned media via western blot (Fig. 6E).

In cell lysates, the wild-type LRP10 protein was detected in both controls and patient-derived astrocytes (Fig. 6E, cell lysates, black arrowheads), and an additional ~ 30 kDa LRP10 species was only detected in cell lysates from the patient P1 and P2 astrocytes (Fig. 6E, cell lysates, pink arrowheads). This observation is in line with the predicted size of the truncated protein that results from the mutant allele. Conditioned media were fractionated into EVs and supernatant fractions as described earlier (Supplementary Fig. 1A). EVs isolated from media that had not been in contact with cells (“–”) did not show the presence of CD63 and CD81 (Fig. 6E, EVs), suggesting the lack of EVs. This sample and EVs isolated from LRP10^{KO} cells were used to distinguish LRP10 signal from non-specific binding of the antibody (Fig. 6E, EVs and Supernatant, asterisks). Interestingly, although LRP10^{WT} was found in the EVs fraction of both control and patient cells (Fig. 6E, EVs, black arrowheads), an additional high molecular weight LRP10

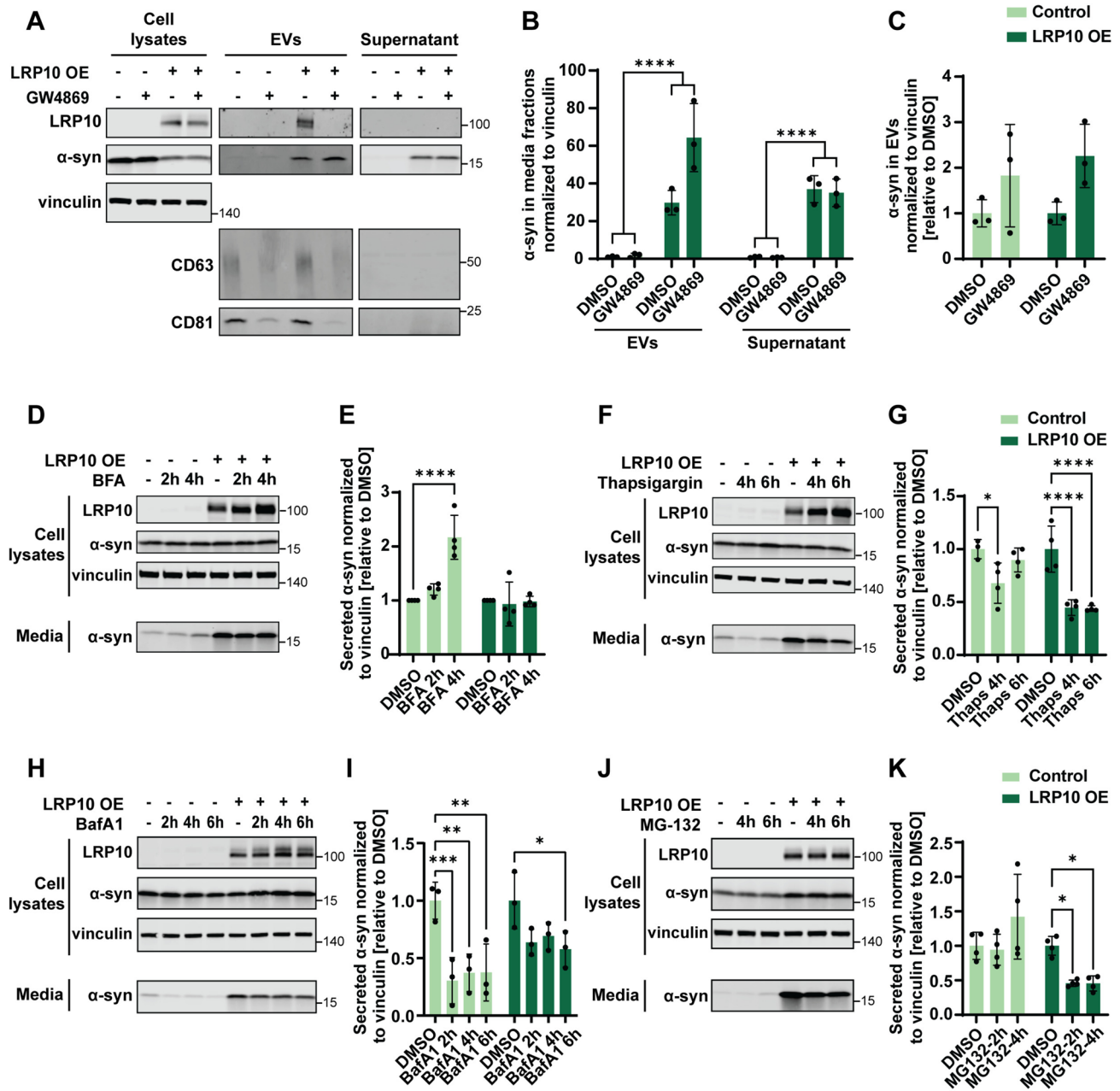


Fig. 5 LRP10-mediated α -synuclein secretion mechanisms. **A** Representative western blot of cell lysates and media fractions (EVs and Supernatant) from 48 h DMSO or GW4869-treated LRP10 and α -synuclein-overexpressing cells. **B, C** Western blot quantifications of α -synuclein from EVs and Supernatant fractions normalised to vinculin (**B**) and α -synuclein from the EVs fraction normalised to vinculin relative to DMSO-treated conditions (**C**). $N=3$ biological replicates. **D–K** Representative western blots and quantifications of LRP10 and α -synuclein-overexpressing cells treated with BFA (4 h

secretion in total; **D, E**), Thapsigargin (6 h secretion in total; **F, G**), BafA1 (6 h secretion in total; **H, I**), and MG-132 (6 h secretion in total; **J, K**). $N=3$ or 4 biological replicates. All data are expressed as mean \pm SD with individual data points shown. Data in **B, C** were analysed by Two-way ANOVA. Data in **E, G, K** were analysed by Two-way ANOVA with Sidak’s multiple comparisons test. Data in **I** were analysed by Two-way ANOVA with Dunnett’s multiple comparisons test. * $P \leq 0.05$, ** $P \leq 0.01$, *** $P \leq 0.001$, **** $P \leq 0.0001$

species was detected in EVs derived from patient cells (Fig. 6E, EVs, pink arrowheads). Strikingly, this additional high molecular weight LRP10 protein could also be detected in the supernatant fraction derived from the patient cells

(Fig. 6E, Supernatant, pink arrowheads). To determine the nature of the novel secreted high molecular weight LRP10 species, we immunoprecipitated LRP10 from the control and patient EVs and Supernatant fractions using an antibody

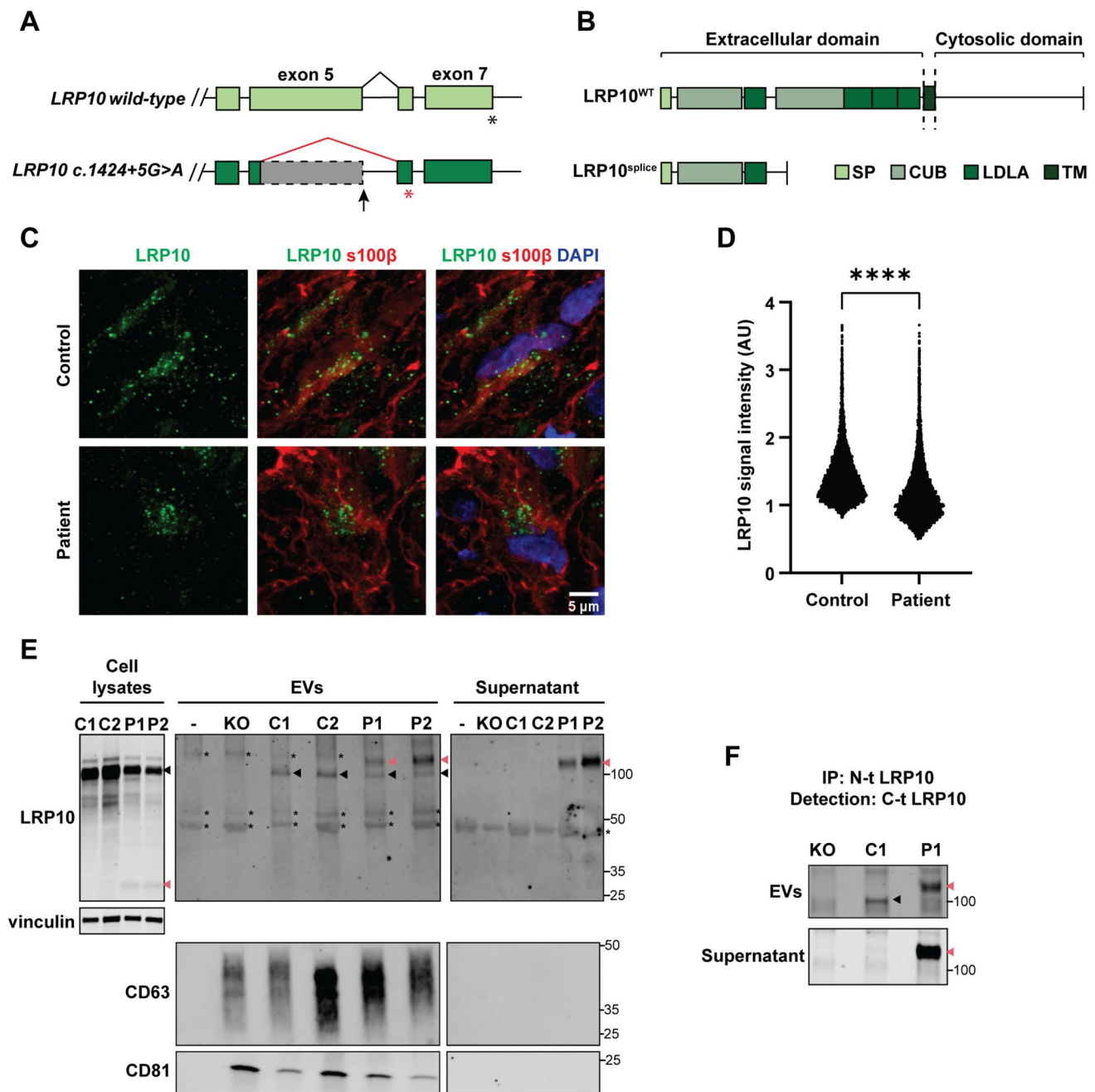


Fig. 6 LRP10 splice variant expression and secretion in patient-derived brain organoids and astrocytes. **A** Schematic of the effect on splicing of the *c.1424+5G>A* *LRP10* variant. **B** Schematic of the result at the protein level of the *c.1424+5G>A* *LRP10* variant (*LRP10*^{splice}). *SP* signaling peptide, *CUB* complement C1r/C1s, Uegf, Bmp1 domain, *LDLA* low-density lipoprotein A domain, *TM* transmembrane. **C** Representative confocal images of LRP10 in s100β-positive astrocytes in control and *LRP10*^{splice} patient-derived brain organoids. **D** Quantification of LRP10 objects signal intensity in s100β-positive astrocytes reported in log scale. $N \geq 8793$ LRP10 objects. **E** Representative western blot of cell lysates, EVs, and

supernatant fractions from *LRP10*^{KO}, control (C1 and C2 lines), and patient iPSC-derived astrocytes (P1 and P2 clones). “—” indicates media that has not been in contact with cells. Black arrowheads indicate full-length LRP10, pink arrowheads indicate aberrant LRP10 species, and “*” indicates non-specific binding. **F** LRP10 pull-down from the EVs and supernatant fractions in **E**. An antibody against the N-terminal domain (*N-t*) of LRP10 was used to immunoprecipitate LRP10, and an antibody against the C-terminal domain (*C-t*) was used for detection. All individual data points are shown. Log-transformed data were analysed by Mann Whitney test. **** $P \leq 0.0001$

against the N-terminal domain (N-t) of full-length LRP10, which binds to both LRP10^{WT} and LRP10^{splice}. For detection of the immunoprecipitated proteins by western blot analysis, an antibody against the C-terminal domain (C-t) of full-length LRP10 was used, which only recognises LRP10^{WT} and not LRP10^{splice}. In both the EVs and supernatant fractions from the patient line (P1), the additional high molecular weight LRP10 protein was detected with the C-t antibody, therefore, confirming the presence of full-length LRP10^{WT} protein in this high molecular weight fragment (Fig. 6F, pink arrowheads). The cause of the increased LRP10 molecular weight is unknown and remains to be determined. A single protein fragment corresponding to the expected LRP10^{WT} molecular weight was observed only in the EVs fraction and not in the Supernatant of the control

cell fractions (Fig. 6F, black arrowhead). In conclusion, LRP10^{splice}-carrying iPSC-derived astrocytes express an additional intracellular ~30 kDa LRP10 species, in addition to a novel secreted LRP10 form of high molecular weight in both EVs and supernatant media fractions.

Overexpressed LRP10^{splice} is localised, secreted, and internalised aberrantly

To further characterise the patient-derived LRP10^{splice}, we generated an overexpression construct consisting of the patient’s mutant cDNA sequence [9] (Supplementary resource 1). We transfected this construct and a plasmid containing LRP10^{WT} in LRP10^{KO} HEK-293T cells and studied their intracellular localisation via immunocytochemistry

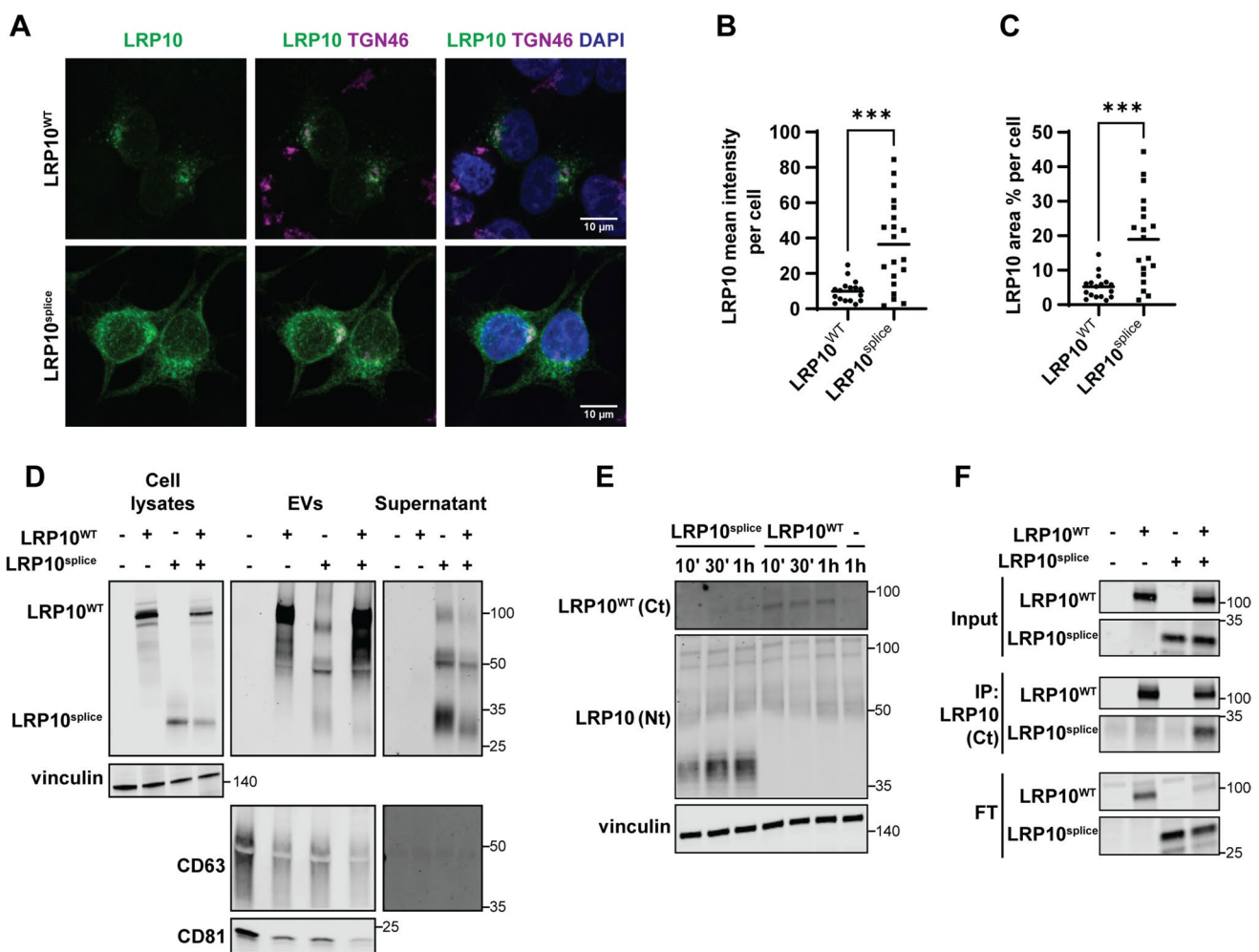


Fig. 7 LRP10^{splice} localisation, secretion, and uptake. **A** Representative confocal images of LRP10^{WT} and LRP10^{splice} in overexpressing LRP10^{KO} HEK-293T cells relative to TGN46. **B, C** Quantifications of LRP10^{WT} and LRP10^{splice} mean signal intensity (**B**) and LRP10 area % (**C**) per cell. *N*=17 and 19 biological replicates, respectively. **D** Representative western blot of cell lysates, EVs, and supernatant fractions from LRP10^{splice}-expressing cells. **E** LRP10^{WT} and LRP10^{splice}

uptake in LRP10^{KO} cells using antibodies against the C-terminal (Ct) and the N-terminal (Nt) domains of LRP10 over time. **F** LRP10 immunoprecipitation with the antibody against the Ct domain of LRP10 that does not bind to LRP10^{splice}. All individual data points are shown including the mean. Data were analysed by unpaired *T*-test. ****P* \leq 0.001

(Fig. 7A). LRP10^{WT} localised to vesicles that clustered around the perinuclear region, and partially colocalised with trans-Golgi network 46 kDa protein (TGN46) [9, 11–14]. However, LRP10^{splice} presented a more intense (Fig. 7B) granular-like pattern distributed around the whole cell cytoplasm (Fig. 7A and C). Next, we investigated intra- and extracellular LRP10^{splice} distribution in cell lysates and conditioned media fractions via western blot (Fig. 7D). In cell lysates, we found an additional ~30 kDa band only in LRP10^{splice}-expressing cells, which was comparable to the molecular weight of the product found in *LRP10 c.1424+5G>A* patient-derived astrocytes (Fig. 6E). In conditioned media, LRP10^{WT} was exclusively detected as a ~100 kDa band in the EVs fraction (Fig. 7D, EVs) as shown previously (Fig. 1B and Supplementary Fig. 1B). In contrast, cells expressing LRP10^{splice} or a combination of LRP10^{splice} and LRP10^{WT} secreted multiple LRP10 species ranging from 28 to 110 kDa in both EVs and supernatant fractions (Fig. 7D, EVs and Supernatant). Therefore, LRP10^{splice} presents a disrupted intracellular localisation pattern and generates an intracellular LRP10 species of similar molecular weight to the one found in patient-derived cells and is aberrantly secreted in both EVs and supernatant fractions in the form of multiple protein fragments of different molecular weights.

As we have demonstrated that LRP10 protein can be internalised via clathrin-mediated endocytosis (Fig. 2), we next investigated LRP10^{splice} uptake in LRP10^{KO} cells. Conditioned media from LRP10^{WT} or LRP10^{splice}-overexpressing cells was placed on LRP10^{KO} cells for 10 min, 30 min, and 1 h before lysing the acceptor cells. We observed that LRP10^{splice} was internalised more efficiently than LRP10^{WT}, which could only be visualised using an antibody against the C-terminal domain of LRP10 (Fig. 7E). Interestingly, internalised LRP10^{splice} consisted of several protein species of different molecular weights ranging from 30 to 40 kDa, and not the original 30 kDa band or the 28–110 kDa bands found in media (Fig. 7D). These observations suggest that LRP10^{splice} is internalised more efficiently than LRP10^{WT} and is processed into 30–40 kDa protein species.

Next, to study whether LRP10^{splice} physically interacts with LRP10^{WT}, we immunoprecipitated LRP10 using an antibody directed against the C-terminal domain of full-length LRP10, which does not recognize LRP10^{splice}. Western blot analysis revealed that LRP10^{splice} co-immunoprecipitates with LRP10^{WT}, demonstrating their physical interaction (Fig. 7F). Taken together, these data indicate that the PD and DLB-associated *LRP10 c.1424+5* variants encode a truncated LRP10^{splice} protein which displays a severely disrupted secretion and internalisation patterns and can physically interact with LRP10^{WT}.

The LRP10 splice variant antagonises the effect of wild-type LRP10 on α -synuclein levels

We next studied the effect of LRP10^{splice} on LRP10-mediated α -synuclein levels fluctuations. To do so, we first transfected LRP10^{KO} HEK-293T cells with *SNCA* and different amounts of LRP10^{WT} and LRP10^{splice} and inspected cell lysates and conditioned media 48 h post-transfection (Fig. 8A). As a result, we observed that LRP10^{splice} overexpression led to a decrease in LRP10^{WT} levels (Fig. 8B), and it counteracted LRP10^{WT}-mediated α -synuclein intracellular levels and secretion (Fig. 8C and D). This effect on α -synuclein secretion was not completely caused by the decrease in LRP10^{WT} levels, since overexpression of α -synuclein and LRP10^{splice} alone in LRP10^{KO} cells led to decreased α -synuclein intracellular levels compared to control cells (Supplementary Fig. 8). Additionally, in contrast to wild-type LRP10, α -synuclein overexpression did not affect LRP10^{splice} levels (Supplementary Fig. 8B). We also studied the effect of LRP10^{splice} expression on α -synuclein levels in later time points. We generated a dox-inducible LRP10^{splice} cell line in LRP10^{KO} HEK-293T cells via antibiotic selection, and kept LRP10^{splice} expression active during the duration of the experiment. α -Synuclein was transfected and intracellular α -synuclein levels were analysed via western blot 72, 96, and 120 h after transfection (Fig. 8E). As a result, we observed that LRP10^{splice} expression led to a significant increase in α -synuclein levels 72 h after transfection (Fig. 8F), in contrast to the previously observed decrease at 48 h (Fig. 8C and Supplementary Fig. 8). Combined, these results suggest a possible dominant negative effect of the LRP10 splice variant.

Discussion

Our findings provide initial functional evidence for the role of LRP10 in LBDs. We first show proof for a potential mechanism that leads to the non-cell-autonomous origin of LRP10 in Lewy bodies, which is based on LRP10 secretion from astrocyte-derived EVs, and subsequent uptake and accumulation in neurons under cellular stress conditions. Furthermore, we demonstrate that LRP10 changes α -synuclein intracellular levels and strongly induces α -synuclein secretion in an ER and proteasome-dependent manner. Additionally, we characterised the patient-derived LRP10^{splice} variant, and we show that it presents abnormal localisation, secretion, and uptake patterns. Finally, our findings indicate that the LRP10^{splice} variant behaves in a dominant negative fashion towards the effect of wild-type LRP10 on intra- and extracellular α -synuclein levels.

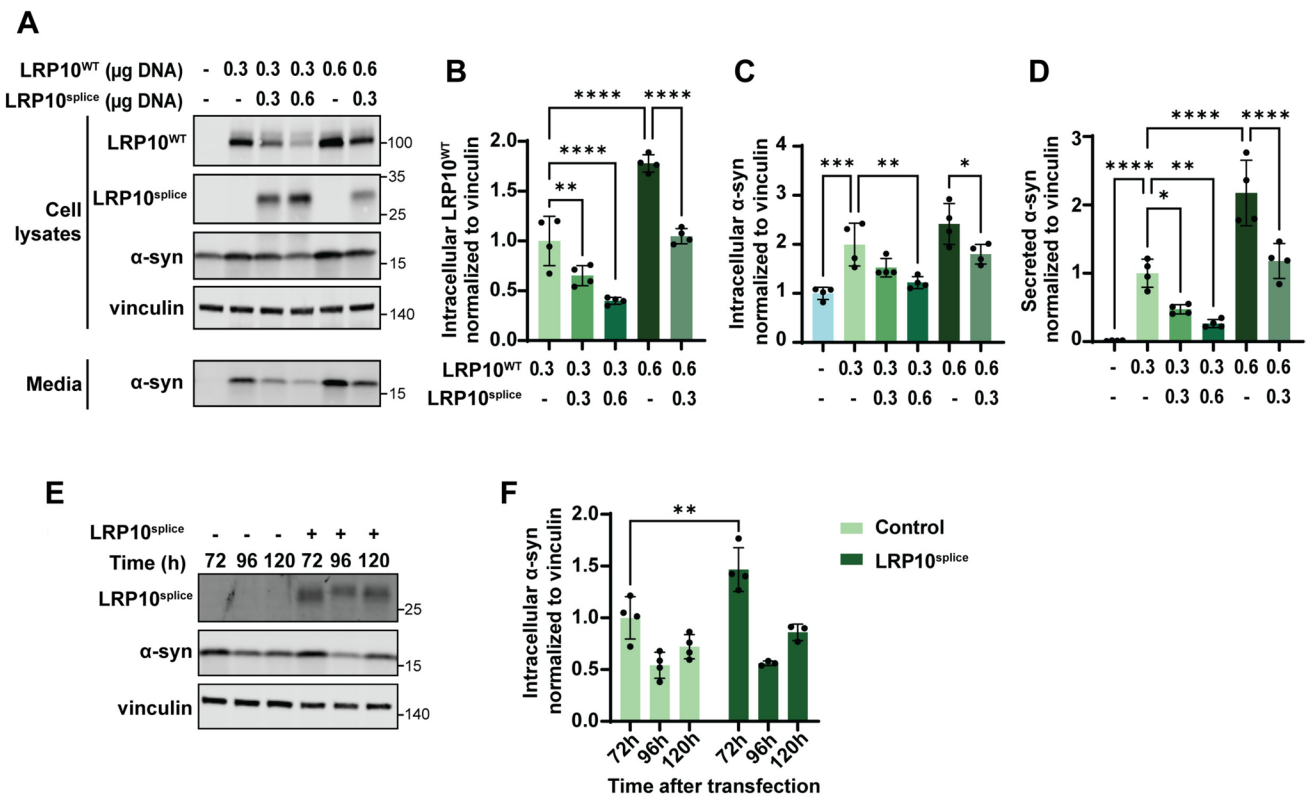


Fig. 8 Effect of LRP10^{splice} on the LRP10^{WT}- α -synuclein interplay. **A** Representative western blot of cell lysates and conditioned media from LRP10^{WT}, LRP10^{splice}, and α -synuclein-overexpressing cells. **B–D** Western blot quantifications of intracellular LRP10^{WT} (**B**) and intracellular (**C**) or extracellular α -synuclein (**D**) normalised to vinculin. *N*=4 biological replicates. **E** Representative western blot of LRP10^{splice} and α -synuclein-overexpressing cells over time. **F** Quan-

tification of intracellular α -synuclein normalised to vinculin at 72, 96, and 120 h after α -synuclein transfection. LRP10^{splice} expression was kept active via Doxycycline treatment every 2 days. *N*=4 biological replicates. All data are expressed as mean \pm SD with individual data points shown. Data were analysed by Two-way ANOVA with Sidak’s multiple comparisons test. **P*≤0.05, ***P*≤0.01, ****P*≤0.001, *****P*≤0.0001

LRP10 is a distant member of the LDLR family [10]. Interestingly, some members of this family, namely LDLR, LRP1, LRP1B, LRP4, and SORL1, have been identified as key players in different neurodegenerative diseases [65–71]. Particularly, LRP1 was recently identified to regulate the transmission of tau and α -synuclein in human neurons in vitro and in mice [66–68]. On another note, LRP10 has been shown to physically interact with SORL1, which suggests that they might function together in a cellular context. Given the fact that both LRP10 and LRP1 have strong effects on α -synuclein secretion, it is, therefore, possible that LRP1 and LRP10 have coordinated roles in α -synuclein transmission, perhaps through physical interaction, for which additional research is required.

LRP10 was found in significant amounts in the core of Lewy bodies in LBD patients, even though it was almost undetectable in control neurons [11]. This observation raised the question of whether, under pathological conditions, LRP10 is secreted from surrounding cells and taken up and accumulated in neurons. In this work, we show that LRP10 is efficiently secreted from overexpressing HEK-293T cells

and control astrocytes via EVs (Figs. 1A–D, J, 6E, 7D, and Supplementary Fig. 1B). EVs are essential in transcellular material transfer and cellular communication, for instance, between astrocytes and neurons [72]. Under pathological conditions, EVs contents have been shown to change [73], and they have even been suggested to promote disease spread [64, 74–76]. Since the current work focuses on LRP10 secretion in vitro, follow-up studies with patient brain material will be essential to clarify whether LRP10 dosage and structure differ in EVs from LBD patients when compared to controls, and if it may influence disease progression. In addition to generating valuable knowledge about disease pathogenesis, it would represent a potential biomarker, since EVs are easily detected in blood and cerebrospinal fluid (CSF) [77].

In addition to being linked to EVs, we show that LRP10 secretion is promoted after inducing autophagic dysfunction (Fig. 1E–L). Particularly, BafA1-treated astrocytes secrete higher levels of LRP10 in whole media but also in EVs (Fig. 1J–L). It has been previously described that inhibition of the autophagy-lysosome degradation pathway can trigger protein secretion through EVs as a compensatory mechanism

to dispose of cellular material, including α -synuclein [63, 78, 79]. Therefore, LRP10 secretion via EVs possibly becomes exacerbated when its degradation via the lysosome-autophagy pathway is impaired via similar mechanisms. In this work, we also show that BafA1 treatment in brain organoids induces the formation of LRP10-positive objects in neurons (Fig. 3F and G). Since LRP10 expression in neurons is very low and the treatment duration was only of 4 h, we believe the origin of these neuronal LRP10 structures not only consists of an accumulation of endogenous LRP10. Alternatively, BafA1 treatment might induce LRP10 secretion from nearby cells (e.g., astrocytes), which is subsequently internalised by these neurons. Given that defects in autophagy are very well described in LBDs [62], it is possible that pre-existing defects in degradation pathways or other cellular stresses trigger LRP10 accumulation in Lewy bodies in both idiopathic and genetic LBD cases. We also hypothesise that, in patients carrying pathogenic *LRP10* variants, the initial trigger for cellular stress might be the presence of abnormal LRP10 species. However, it is yet to be determined whether wild-type or mutant LRP10 play an active role in Lewy body formation and maturation or if LRP10 localisation in Lewy bodies is a secondary effect of the disease.

In healthy brains and brain organoids, LRP10 expression is higher in astrocytes than in neurons [11, 55–57] (Fig. 3A and B). A growing amount of evidence supports the essential role of astrocytes in LBD pathogenesis. Astrocytes are central in keeping brain homeostasis and perform essential functions such as the secretion of survival factors and synapse regulation in neurons and maintaining the blood–brain barrier [80–83]. In PD and other neurodegenerative disorders, astrocytes have been proven inefficient in their neuronal-supporting role, in addition to inducing neuroinflammation [84–86]. Besides *LRP10*, several other LBD genes, including *DJ-1*, *PINK1*, and *GBA1*, are highly expressed in astrocytes, and the encoding proteins have been shown to have a role in astrocyte biology [55, 87–91]. Moreover, disease-linked genetic variants have been shown to interfere with their normal function and contribute to disease progression [87, 91–93]. Additional research will clarify the role of LRP10 in astrocytic function, and whether it is impaired in *LRP10*-variant-carrying patients.

Our findings show that LRP10 overexpression leads to time-dependent changes in α -synuclein intracellular levels (Fig. 4). Additionally, we show that α -synuclein overexpression leads to a decrease in LRP10 levels (Fig. 4A and B). Similar feedback loops have been described before between α -synuclein and LBD-linked proteins, such as *GBA* [94]. α -Synuclein is considered to be central in LBDs, and a key defining feature of Lewy bodies, but whether and how α -synuclein initiates the disease cascade in all patients remains unclear. Moreover, even though the

majority of LBD research has focused on the detrimental effect of α -synuclein, several arguments challenge this hypothesis. For instance, triple synuclein KO mice present neuropathological defects and reduced survival [95, 96]. Therefore, proteins that regulate α -synuclein levels may provide relevant insight into α -synuclein biology and its role in disease initiation and progression. Furthermore, even though a myriad of α -synuclein species has been described, clear evidence for their significance in pathology is lacking for the majority of them [32]. In contrast to α -synuclein oligomers, which have a well-documented neurotoxic effect, this work focuses on monomeric α -synuclein, with a poorly understood pathogenic role [32, 97]. However, several modifications on α -synuclein monomers are associated with increased misfolding and aggregation potential [32, 34, 98]. Additionally, increased *SNCA* dosage leads to a strong neuropathological phenotype, also in humans carrying gene multiplications [99, 100]. All in all, α -synuclein pathology in LBDs remains incompletely understood, to a great extent due to the fact that experimental models to study LBDs show limited capacity to recapitulate α -synuclein pathology. Highly valuable insight has been obtained from studies performed in animal models using transgenic expression of human α -synuclein, overexpression, or addition of pre-formed α -synuclein fibrils [101]. Furthermore, cellular models have the capacity to mimic certain traits of human disease and are useful to study patient-derived genetic variations, but studies that focus on α -synuclein pathology also heavily rely on enhancing pathological α -synuclein levels [102]. Furthermore, many LBD patients suffer from late-onset forms of the disease, which hinders the study of endogenous pathology in differentiated patient-derived iPSC cell lines, which are known to have an expression profile that resembles that of an embryonic state rather than that of a mature state [103]. In this work, our model to study LRP10 and α -synuclein has important limitations, including overexpression, the use of non-neural cell lines, and the lack of the aging component of LBDs, among others, but provides important initial mechanistic evidence for the interplay between these two proteins that should be further explored, and could greatly benefit from the use of more physiological disease models.

In this study, we show that LRP10 overexpression also induces a strong increase in α -synuclein secretion (Figs. 4 and 5). Interestingly, LRP12, another distant relative of the LDLR family, was also found to modify α -synuclein cell-to-cell transfer in vitro [104]. α -Synuclein transmission is currently considered to be central in disease pathogenesis and progression [29]. Oligomeric α -synuclein is detected in CSF and it has been proposed as a biomarker for PD [105]. Therefore, LRP10-mediated α -synuclein secretion might have diagnostic potential for *LRP10*-variant-carrying patients, although it is not yet clear if these patients present a loss or

gain of LRP10 function. α -Synuclein has been shown to be secreted via several unconventional pathways [63, 64, 78, 79]. Here, we demonstrate that LRP10 induces α -synuclein secretion via cell-stress response pathways, including ER stress and the proteasome (Fig. 5F, G, J, and K). In line with this observation, several studies show that α -synuclein aggregates or overexpression lead to defects in proteasomal function [106–108]. Interestingly, certain cellular sensors that are able to detect misfolded proteins have been shown to induce proteasome-dependent secretion of these proteins [109]. Taking this into account, it is possible that LRP10 is acting as a sensor of α -synuclein overexpression and exporting misfolded proteins through a novel unconventional α -synuclein secretion pathway.

The present work focuses on studying the overexpression of LRP10 and α -synuclein simultaneously in the same cells. As previously discussed, LRP10 is enriched in astrocytes in comparison to neurons, whereas α -synuclein is typically considered to be a neuronal protein. To explain the interaction between LRP10 and α -synuclein, a multicellular model is required. One possible hypothesis is that LRP10 regulates α -synuclein in a later disease state within neurons after LRP10 internalisation. Another possibility is that LRP10 levels affect α -synuclein processing within astrocytes, which, in LRP10-variants-carrying patients, might play a role in disease initiation. Increasing evidence suggests that astrocytes play a more important role in α -synuclein pathology than what was initially considered. Recent work from Altay et al. [110] described that astrocytic α -synuclein accumulations present unique post-translational modifications, and colocalise with different markers when compared to neuronal α -synuclein-positive inclusions. For this reason, on many occasions, astrocytic α -synuclein is not detected with antibodies that recognize α -synuclein in neuronal Lewy bodies. In agreement, several reports show different types of α -synuclein accumulations in astrocytes in patient post-mortem material [111–120]. Furthermore, pathological α -synuclein has been shown to dysregulate essential functions in astrocytes [87, 92, 121–123], and, in turn, astrocytes have been shown to spread α -synuclein pathology to neurons [84, 124]. Taken together, the present study demonstrates a functional link between LRP10 and α -synuclein, but the biological context where this interaction takes place possibly involves several cell types and remains of difficult interpretation.

Finally, we show several defects associated with the LRP10 splice variant identified in PD and DLB patients (Figs. 6, 7, 8). First, we observe differences in LRP10 localisation in LRP10^{splice} brain organoids, since LRP10 signal is reduced within s100 β -positive astrocytes as determined by immunocytochemistry (Fig. 6C and D), but not in total protein lysates from brain organoids as determined by WB (Supplementary Fig. 6B and 6C). Next, we show that

patient-derived cells secrete an aberrant patient-specific high molecular weight LRP10 species (Fig. 6E). Interestingly, this high molecular weight form of LRP10 is not found intracellularly, pointing towards a patient-specific mechanism occurring during secretion. Crucially, we show that this patient-specific extracellular LRP10 species contains wild-type LRP10 (Fig. 6F), but it is not found in control cells. Given the size of this aberrant extracellular LRP10 form on SDS-page gels (Fig. 6E and F), one possibility might be that LRP10^{splice} forms SDS-resistant protein oligomers with LRP10^{WT}. In line with this hypothesis, it has been described that LRP6 forms SDS-resistant homodimers via its LDLA domain to be functionally active as a co-receptor for Wnt signalling [125]. It is therefore possible that LRP10 also dimerises via its LDLA domains, which become SDS-resistant due to the molecular properties of the LRP10^{splice} variant. Alternatively, LRP10^{splice} might increase LRP10^{WT} molecular weight by mediating its binding to other proteins or the introduction of post-translational modifications. Furthermore, the fact that LRP10^{WT} is found in the supernatant fraction of the media from patient cells suggests that it is likely not linked to cell membranes, which is striking considering LRP10 is a type-I transmembrane protein [10]. These results suggest that the LRP10^{splice} variant also affects LRP10^{WT} processing, either via proteolytic processing at the plasma membrane or other mechanisms that can dissociate LRP10 from the membrane.

In our overexpression model, LRP10^{splice} shows a different intracellular localisation pattern when compared to LRP10^{WT} (Fig. 7A–C). In contrast to LRP10^{WT}, which presents a vesicular localisation that accumulates predominantly around the nucleus, LRP10^{splice} presents a more intense cytoplasmic distribution with a granular pattern. Furthermore, LRP10^{splice} is secreted in the form of different protein species of higher molecular weight (Fig. 7D). However, extracellular overexpressed LRP10^{splice} cDNA presents a different pattern on SDS-PAGE gels when compared to endogenous expression in the *c.1424+5G>A* LRP10 variant-carrier patient lines (Fig. 6E), suggesting that the LRP10 genetic context in the genome, the LRP10^{WT}—LRP10^{splice} ratio, the expression time, and/or the cell type might play a role in this secretion pattern. Additionally, LRP10^{splice} is found as several protein species of different sizes after uptake, and not the original monomeric 30 kDa form (Fig. 7E). These findings suggest that secreted LRP10 in patients carrying the *c.1424+5G>A* variant might have aggregation potential; an effect that is perhaps not occurring in the donor cells (e.g. astrocytes), but might occur in the acceptor cells (e.g., neurons). Furthermore, we demonstrate that LRP10^{splice} binds to full-length LRP10 (Fig. 7F) and antagonises its effect on α -synuclein levels (Fig. 8A–D), pointing to a dominant-negative effect. Additionally, overexpression of LRP10^{splice} alone in LRP10^{KO} cells affects α -synuclein levels in an

opposite way when compared to LRP10^{WT} (Fig. 8E and F, and Supplementary Fig. 8). Therefore, not only LRP10^{splice} has a dominant negative effect over LRP10^{WT} but might also modulate α -synuclein levels. Overall, we show evidence for the pathological potential of the LRP10 splice variant, which might be disease-causing in these carriers. Additional work remains ahead to further elucidate the consequences of this variant in mutation-carrying patients. For instance, neuropathological examination of these patients remains to be performed. Importantly, different types of *LRP10* variants have been identified to date [9, 16–25]. Due to the nature of these genetic variations they were initially considered to present with a loss-of-function mechanism of action [9]. However, in light of the findings from this paper regarding the LRP10^{splice} variant, we conclude that each genetic variation might affect LRP10 function in different ways, which remains to be investigated. Therefore, too little is known to provide a direct link between *LRP10* genetic variants and α -synuclein pathology in general.

In conclusion, this work provides initial evidence for the non-cell autonomous origin of LRP10 in Lewy bodies, in addition to a possible functional role of LRP10 in LBDs via affecting α -synuclein levels, and shows pathogenic mechanisms linked to the patient-associated *c.1424+5G>A* *LRP10* variant.

Supplementary Information The online version contains supplementary material available at <https://doi.org/10.1007/s00018-024-05135-0>.

Acknowledgements We thank the donors and their families for making this study possible. We also thank Erasmus MC iPSC Core Facility for providing the human iPSC lines.

Author Contributions ACM, MMG, MEvR, and WM designed the experiments. ACM, MMG, VaB, ENB, GJB, NFJD, and MEvR performed the experiments. ACM, MMG, VaB, NFJD, and MEvR performed data analysis. ACM, MMG, VaB, NFJD, MEvR, VB, and WM interpreted the data. LV and FJdJ provided the patient biopsy. ACM wrote the initial draft of the manuscript. VB and WM conceived the study and supervised the experiments. All authors critically read the manuscript and approved the final version.

Funding This work was supported by research grants from the Stichting ParkinsonFonds (The Netherlands) and from Alzheimer Nederland to VB and from the Stichting ParkinsonFonds (The Netherlands) to WM.

Availability of data and materials The data that support the findings of this study are available from the corresponding authors, upon reasonable request.

Declarations

Conflict of interests The authors declare no conflict of interest.

Ethics approval Primary cell lines were obtained within study protocols approved by the medical ethical committee of Erasmus MC and conformed to the principles of the Declaration of Helsinki.

Consent to participate The participating human subjects provided written informed consent for the use of the material for research purposes.

Consent to publish The participating human subjects provided written informed consent for publication.

Open Access This article is licensed under a Creative Commons Attribution 4.0 International License, which permits use, sharing, adaptation, distribution and reproduction in any medium or format, as long as you give appropriate credit to the original author(s) and the source, provide a link to the Creative Commons licence, and indicate if changes were made. The images or other third party material in this article are included in the article's Creative Commons licence, unless indicated otherwise in a credit line to the material. If material is not included in the article's Creative Commons licence and your intended use is not permitted by statutory regulation or exceeds the permitted use, you will need to obtain permission directly from the copyright holder. To view a copy of this licence, visit <http://creativecommons.org/licenses/by/4.0/>.

References

- Attems J, Toledo JB, Walker L, Gelpi E, Gentleman S, Halliday G et al (2021) Neuropathological consensus criteria for the evaluation of Lewy pathology in post-mortem brains: a multi-centre study. *Acta Neuropathol* 141(2):159–172
- Feigin VL, Nichols E, Alam T, Bannick MS, Beghi E, Blake N et al (2019) Global, regional, and national burden of neurological disorders, 1990–2016: a systematic analysis for the Global Burden of Disease Study 2016. *Lancet Neurol* 18(5):459–480
- Hogan DB, Fiest KM, Roberts JI, Maxwell CJ, Dykeman J, Pringsheim T et al (2016) The prevalence and incidence of dementia with lewy bodies: a systematic review. *Can J Neurol Sci* 43(S1):S83–S95
- Nalls MA, Duran R, Lopez G, Kurzawa-Akanbi M, McKeith IG, Chinnery PF et al (2013) A multicenter study of glucocerebrosidase mutations in dementia with Lewy bodies. *JAMA Neurol* 70(6):727–735
- Konno T, Ross OA, Puschmann A, Dickson DW, Wszolek ZK (2016) Autosomal dominant Parkinson's disease caused by SNCA duplications. *Parkinsonism Relat Disord* 22:S1–S6
- Guerreiro R, Ross OA, Kun-Rodrigues C, Hernandez DG, Orme T, Eicher JD et al (2018) Investigating the genetic architecture of dementia with Lewy bodies: a two-stage genome-wide association study. *Lancet Neurol* 17(1):64–74
- Sidransky E, Lopez G (2012) The link between the GBA gene and parkinsonism. *Lancet Neurol* 11(11):986–998
- Sanghvi H, Singh R, Morrin H, Rajkumar AP (2020) Systematic review of genetic association studies in people with Lewy body dementia. *Int J Geriatr Psychiatry* 35(5):436–448
- Quadri M, Mandemakers W, Grochowska MM, Masius R, Geut H, Fabrizio E et al (2018) LRP10 genetic variants in familial Parkinson's disease and dementia with Lewy bodies: a genome-wide linkage and sequencing study. *Lancet Neurol* 17(7):597–608
- Pohlkamp T, Wasser CR, Herz J (2017) Functional roles of the interaction of APP and lipoprotein receptors. *Front Mol Neurosci*. <https://doi.org/10.3389/fnmol.2017.00054>
- Grochowska MM, Carreras Mascaró A, Boumeester V, Natale D, Breedveld GJ, Geut H et al (2021) LRP10 interacts with SORL1 in the intracellular vesicle trafficking pathway in non-neuronal brain cells and localises to Lewy bodies in Parkinson's disease and dementia with Lewy bodies. *Acta Neuropathol* 142(1):117–137

12. Brodeur J, Larkin H, Boucher R, Thériault C, St-Louis SC, Gagnon H et al (2009) Calnexin binds to LRP9 and affects its endosomal sorting. *Traffic* 10(8):1098–1114
13. Doray B, Knisely JM, Wartman L, Bu G, Kornfeld S (2008) Identification of acidic dileucine signals in LRP9 that interact with both GGAs and AP-1/AP-2. *Traffic* 9(9):1551–1562
14. Boucher R, Larkin H, Brodeur J, Gagnon H, Thériault C, Lavoie C (2008) Intracellular trafficking of LRP9 is dependent on two acidic cluster/dileucine motifs. *Histochem Cell Biol* 130(2):315–327
15. Steinberg F, Gallon M, Winfield M, Thomas EC, Bell AJ, Heesom KJ et al (2013) A global analysis of SNX27-retromer assembly and cargo specificity reveals a function in glucose and metal ion transport. *Nat Cell Biol* 15(5):461–471
16. Vergouw LJM, Ruitenbergh A, Wong TH, Melhem S, Breedveld GJ, Criscuolo C et al (2019) LRP10 variants in Parkinson's disease and dementia with Lewy bodies in the South-West of the Netherlands. *Parkinsonism Relat Disord* 65:243–247
17. Vergouw LJM, Geut H, Breedveld G, Kuipers DJS, Quadri M, Netherlands Brain B et al (2020) Clinical and pathological phenotypes of LRP10 variant carriers with dementia. *J Alzheimers Dis* 76(3):1161–1170
18. Chen Y, Cen Z, Zheng X, Pan Q, Chen X, Zhu L et al (2019) LRP10 in autosomal-dominant Parkinson's disease. *Mov Disord* 34(6):912–916
19. Zhao Y, Qin L, Pan H, Liu Z, Jiang L, He Y et al (2020) The role of genetics in Parkinson's disease: a large cohort study in Chinese mainland population. *Brain* 143(7):2220–2234
20. Zhao Q, Ning P, Yang X, Shi C, Xu Y, Shen Q et al (2021) LRP10 mutations may correlate with sporadic Parkinson's disease in China. *Mol Neurobiol* 58(3):1212–1216
21. Li C, Chen Y, Ou R, Gu X, Wei Q, Cao B et al (2021) Mutation analysis of LRP10 in a large Chinese familial Parkinson disease cohort. *Neurobiol Aging* 99(99):e1–e6
22. Song N, Wang Y, Zhou L, Zhang J, Wu F, Li M et al (2022) Genetic analysis of the LRP10 gene in Chinese patients with Parkinson's disease. *Neurol Sci*. <https://doi.org/10.1007/s10072-022-06496-9>
23. Tan MMX, Malek N, Lawton MA, Hubbard L, Pittman AM, Joseph T et al (2019) Genetic analysis of Mendelian mutations in a large UK population-based Parkinson's disease study. *Brain* 142(9):2828–2844
24. Vergouw LJM, Melhem S, Donker Kaat L, Chiu WZ, Kuipers DJS, Breedveld G et al (2020) LRP10 variants in progressive supranuclear palsy. *Neurobiol Aging* 94:311.e5–e.10
25. Ni J, Liu Z, Li W, Yuan Y, Huang L, Hu Y et al (2021) Rare, pathogenic variants in LRP10 are associated with amyotrophic lateral sclerosis in patients from mainland China. *Neurobiol Aging* 97:145.e17–e22
26. Brodeur J, Thériault C, Lessard-Beaudoin M, Marciel A, Dahan S, Lavoie C (2012) LDLR-related protein 10 (LRP10) regulates amyloid precursor protein (APP) trafficking and processing: evidence for a role in Alzheimer's disease. *Mol Neurodegener* 7:31
27. Sugiyama T, Kumagai H, Morikawa Y, Wada Y, Sugiyama A, Yasuda K et al (2000) A novel low-density lipoprotein receptor-related protein mediating cellular uptake of apolipoprotein E-enriched beta-VLDL in vitro. *Biochemistry* 39(51):15817–15825
28. Neff RA, Wang M, Vatansever S, Guo L, Ming C, Wang Q et al (2021) Molecular subtyping of Alzheimer's disease using RNA sequencing data reveals novel mechanisms and targets. *Sci Adv*. <https://doi.org/10.1126/sciadv.abb5398>
29. Peng C, Trojanowski JQ, Lee VMY (2020) Protein transmission in neurodegenerative disease. *Nat Rev Neurol* 16(4):199–212
30. Iwai A, Masliah E, Yoshimoto M, Ge N, Flanagan L, Rohan de Silva HA et al (1995) The precursor protein of non-A β component of Alzheimer's disease amyloid is a presynaptic protein of the central nervous system. *Neuron* 14(2):467–475
31. Burré J, Sharma M, Tsetsenis T, Buchman V, Etherton MR, Südhof TC (2010) Alpha-synuclein promotes SNARE-complex assembly in vivo and in vitro. *Science* 329(5999):1663–1667
32. Burré J, Sharma M, Südhof TC (2018) Cell biology and pathophysiology of α -synuclein. *Cold Spring Harbor Perspect Med* 8(3):a024091
33. Clayton DF, George JM (1998) The synucleins: a family of proteins involved in synaptic function, plasticity, neurodegeneration and disease. *Trends Neurosci* 21(6):249–254
34. Zhang S, Zhu R, Pan B, Xu H, Olufemi MF, Gathagan RJ et al (2023) Post-translational modifications of soluble α -synuclein regulate the amplification of pathological α -synuclein. *Nat Neurosci* 26:2250
35. So RWL, Watts JC (2023) α -Synuclein conformational strains as drivers of phenotypic heterogeneity in neurodegenerative diseases. *J Mol Biol* 435:168011
36. Luk KC, Song C, O'Brien P, Stieber A, Branch JR, Brunden KR et al (2009) Exogenous alpha-synuclein fibrils seed the formation of Lewy body-like intracellular inclusions in cultured cells. *Proc Natl Acad Sci U S A* 106(47):20051–20056
37. Volpicelli-Daley LA, Luk KC, Patel TP, Tanik SA, Riddle DM, Stieber A et al (2011) Exogenous α -synuclein fibrils induce Lewy body pathology leading to synaptic dysfunction and neuron death. *Neuron* 72(1):57–71
38. Peng C, Gathagan RJ, Covell DJ, Medellín C, Stieber A, Robinson JL et al (2018) Cellular milieu imparts distinct pathological α -synuclein strains in α -synucleinopathies. *Nature* 557(7706):558–563
39. Braak H, Del Tredici K, Rüb U, de Vos RA, Jansen Steur EN, Braak E (2003) Staging of brain pathology related to sporadic Parkinson's disease. *Neurobiol Aging* 24(2):197–211
40. Sacino AN, Brooks M, Thomas MA, McKinney AB, Lee S, Regenhardt RW et al (2014) Intramuscular injection of α -synuclein induces CNS α -synuclein pathology and a rapid-onset motor phenotype in transgenic mice. *Proc Natl Acad Sci U S A* 111(29):10732–10737
41. Breid S, Bernis ME, Babila JT, Garza MC, Wille H, Tamgüney G (2016) Neuroinvasion of α -synuclein prionoids after intraperitoneal and intraglossal inoculation. *J Virol* 90(20):9182–9193
42. Ayers JI, Brooks MM, Rutherford NJ, Howard JK, Sorrentino ZA, Riffe CJ et al (2017) Robust central nervous system pathology in transgenic mice following peripheral injection of α -synuclein fibrils. *J Virol* 91(2):e02095
43. Uemura N, Yagi H, Uemura MT, Hatanaka Y, Yamakado H, Takahashi R (2018) Inoculation of α -synuclein preformed fibrils into the mouse gastrointestinal tract induces Lewy body-like aggregates in the brainstem via the vagus nerve. *Mol Neurodegener* 13(1):21
44. Grochowska MM, Bonifati V, Mandemakers W (2022) CRISPR/Cas9-mediated LRP10 Knockout in HuTu-80 and HEK 293T Cell Lines. *Bio-Protoc* 12(19):e4521
45. Cowan CA, Klimanskaya I, McMahon J, Atienza J, Witmyer J, Zucker JP et al (2004) Derivation of embryonic stem-cell lines from human blastocysts. *N Engl J Med* 350(13):1353–1356
46. Mandegar MA, Huebsch N, Frolov EB, Shin E, Truong A, Olvera MP et al (2016) CRISPR interference efficiently induces specific and reversible gene silencing in human iPSCs. *Cell Stem Cell* 18(4):541–553
47. Vanhauwaert R, Kuenen S, Masius R, Bademosi A, Manetsberger J, Schoovaerts N et al (2017) The SAC1 domain in synaptojanin is required for autophagosome maturation at presynaptic terminals. *Embo J* 36(10):1392–1411

48. Barakat TS, Ghazvini M, de Hoon B, Li T, Eussen B, Douben H et al (2015) Stable X chromosome reactivation in female human induced pluripotent stem cells. *Stem cell reports* 4(2):199–208
49. Reinhardt P, Glatz M, Hemmer K, Tsytsyura Y, Thiel CS, Höing S et al (2013) Derivation and expansion using only small molecules of human neural progenitors for neurodegenerative disease modeling. *PLoS ONE* 8(3):e59252-e
50. Renner H, Grabos M, Becker KJ, Kagermeier TE, Wu J, Otto M et al (2020) A fully automated high-throughput workflow for 3D-based chemical screening in human midbrain organoids. *Elife* 9:e52904
51. Monzel AS, Smits LM, Hemmer K, Hachi S, Moreno EL, van Wuellem T et al (2017) Derivation of human midbrain-specific organoids from neuroepithelial stem cells. *Stem Cell Rep* 8(5):1144–1154
52. Lee BR, Kamitani T (2011) Improved immunodetection of endogenous α -synuclein. *PLoS ONE* 6(8):e23939
53. Hartjes TA, Slotman JA, Vredendregt MS, Dits N, Van der Meel R, Duijvesz D et al (2020) EVQuant; high-throughput quantification and characterization of extracellular vesicle (sub)populations. *bioRxiv*. <https://doi.org/10.1101/2020.10.21.348375>
54. Théry C, Witwer KW, Aikawa E, Alcaraz MJ, Anderson JD, Andriantsitohaina R et al (2018) Minimal information for studies of extracellular vesicles 2018 (MISEV2018): a position statement of the International Society for Extracellular Vesicles and update of the MISEV2014 guidelines. *J Extracell Vesic* 7(1):1535750
55. Zhang Y, Sloan SA, Clarke LE, Caneda C, Plaza CA, Blumenthal PD et al (2016) Purification and characterization of progenitor and mature human astrocytes reveals transcriptional and functional differences with mouse. *Neuron* 89(1):37–53
56. La Manno G, Gyllborg D, Codeluppi S, Nishimura K, Salto C, Zeisel A et al (2016) Molecular diversity of midbrain development in mouse, human, and stem cells. *Cell* 167(2):566–80.e19
57. Barbar L, Jain T, Zimmer M, Kruglikov I, Sadick JS, Wang M et al (2020) CD49f is a novel marker of functional and reactive human iPSC-derived astrocytes. *Neuron* 107(3):436–53.e12
58. Macia E, Ehrlich M, Massol R, Boucrot E, Brunner C, Kirchhausen T (2006) Dynasore, a cell-permeable inhibitor of dynamin. *Dev Cell* 10(6):839–850
59. Chaboub LS, Deneen B (2013) Astrocyte form and function in the developing central nervous system. *Semin Pediatr Neurol* 20(4):230–235
60. Kittappa R, Chang WW, Awatramani RB, McKay RD (2007) The *foxa2* gene controls the birth and spontaneous degeneration of dopamine neurons in old age. *PLoS Biol* 5(12):e325
61. Bin JM, Harris SN, Kennedy TE (2016) The oligodendrocyte-specific antibody “CC1” binds Quaking 7. *J Neurochem* 139(2):181–186
62. Hou X, Watzlawik JO, Fiesel FC, Springer W (2020) Autophagy in Parkinson’s disease. *J Mol Biol* 432(8):2651–2672
63. Fussi N, Höllerhage M, Chakroun T, Nykänen NP, Rösler TW, Koeglsperger T et al (2018) Exosomal secretion of α -synuclein as protective mechanism after upstream blockage of macroautophagy. *Cell Death Dis* 9(7):757
64. Emmanouilidou E, Melachroinou K, Roumeliotis T, Garbis SD, Ntzouni M, Margaritis LH et al (2010) Cell-produced α -synuclein is secreted in a calcium-dependent manner by exosomes and impacts neuronal survival. *J Neurosci* 30(20):6838–6851
65. Shi Y, Andhey PS, Ising C, Wang K, Snipes LL, Boyer K et al (2021) Overexpressing low-density lipoprotein receptor reduces tau-associated neurodegeneration in relation to apoE-linked mechanisms. *Neuron* 109(15):2413–26 e7
66. Rauch JN, Luna G, Guzman E, Audouard M, Challis C, Sibih YE et al (2020) LRP1 is a master regulator of tau uptake and spread. *Nature* 580(7803):381–385
67. Cooper JM, Lathuiliere A, Migliorini M, Arai AL, Wani MM, Dujardin S et al (2021) Regulation of tau internalization, degradation, and seeding by LRP1 reveals multiple pathways for tau catabolism. *J Biol Chem* 296:100715
68. Chen K, Martens YA, Meneses A, Ryu DH, Lu W, Raulin AC et al (2022) LRP1 is a neuronal receptor for α -synuclein uptake and spread. *Mol Neurodegener* 17(1):57
69. Zhang H, Chen W, Tan Z, Zhang L, Dong Z, Cui W et al (2020) A role of low-density lipoprotein receptor-related protein 4 (LRP4) in astrocytic A β clearance. *J Neurosci* 40(28):5347–5361
70. Rogaeva E, Meng Y, Lee JH, Gu Y, Kawarai T, Zou F et al (2007) The neuronal sortilin-related receptor SORL1 is genetically associated with Alzheimer disease. *Nat Genet* 39(2):168–177
71. Real R, Martinez-Carrasco A, Reynolds RH, Lawton MA, Tan MMX, Shoai M et al (2022) Association between the LRP1B and APOE loci in the development of Parkinson’s disease dementia. *Brain* 146:1873–1887
72. Chun C, Smith AST, Kim H, Kamenz DS, Lee JH, Lee JB et al (2021) Astrocyte-derived extracellular vesicles enhance the survival and electrophysiological function of human cortical neurons in vitro. *Biomaterials* 271:120700
73. Shi M, Liu C, Cook TJ, Bullock KM, Zhao Y, Gingham C et al (2014) Plasma exosomal α -synuclein is likely CNS-derived and increased in Parkinson’s disease. *Acta Neuropathol* 128(5):639–650
74. Hill AF (2019) Extracellular vesicles and neurodegenerative diseases. *J Neurosci* 39(47):9269–9273
75. Stuenkel A, Kunadt M, Kruse N, Bartels C, Moebius W, Danzer KM et al (2016) Induction of α -synuclein aggregate formation by CSF exosomes from patients with Parkinson’s disease and dementia with Lewy bodies. *Brain* 139(Pt 2):481–494
76. Danzer KM, Kranich LR, Ruf WP, Cagsal-Getkin O, Winslow AR, Zhu L et al (2012) Exosomal cell-to-cell transmission of alpha synuclein oligomers. *Mol Neurodegener* 7:42
77. Boukouris S, Mathivanan S (2015) Exosomes in bodily fluids are a highly stable resource of disease biomarkers. *Proteomics Clin Appl* 9(3–4):358–367
78. Alvarez-Erviti L, Seow Y, Schapira AH, Gardiner C, Sargent IL, Wood MJ et al (2011) Lysosomal dysfunction increases exosome-mediated alpha-synuclein release and transmission. *Neurobiol Dis* 42(3):360–367
79. Minakaki G, Menges S, Kittel A, Emmanouilidou E, Schaeffner I, Barkovits K et al (2018) Autophagy inhibition promotes SNCA/alpha-synuclein release and transfer via extracellular vesicles with a hybrid autophagosome-exosome-like phenotype. *Autophagy* 14(1):98–119
80. Sofroniew MV, Vinters HV (2010) Astrocytes: biology and pathology. *Acta Neuropathol* 119(1):7–35
81. Banker GA (1980) Trophic interactions between astroglial cells and hippocampal neurons in culture. *Science* 209(4458):809–810
82. Allen NJ, Eroglu C (2017) Cell biology of astrocyte–synapse interactions. *Neuron* 96(3):697–708
83. Abbott NJ, Rönnbäck L, Hansson E (2006) Astrocyte-endothelial interactions at the blood-brain barrier. *Nat Rev Neurosci* 7(1):41–53
84. di Domenico A, Carola G, Calatayud C, Pons-Espinal M, Muñoz JP, Richaud-Patin Y et al (2019) Patient-specific iPSC-derived astrocytes contribute to non-cell-autonomous neurodegeneration in Parkinson’s disease. *Stem Cell Rep* 12(2):213–229
85. Maragakis NJ, Rothstein JD (2006) Mechanisms of disease: astrocytes in neurodegenerative disease. *Nat Clin Pract Neurol* 2(12):679–689
86. Liddel SA, Guttenplan KA, Clarke LE, Bennett FC, Bohlen CJ, Schirmer L et al (2017) Neurotoxic reactive astrocytes are induced by activated microglia. *Nature* 541(7638):481–487

87. Booth HDE, Hirst WD, Wade-Martins R (2017) The role of astrocyte dysfunction in Parkinson's disease pathogenesis. *Trends Neurosci* 40(6):358–370
88. Kim J-M, Cha S-H, Choi YR, Jou I, Joe E-H, Park SM (2016) DJ-1 deficiency impairs glutamate uptake into astrocytes via the regulation of flotillin-1 and caveolin-1 expression. *Sci Rep* 6(1):28823
89. Bandopadhyay R, Kingsbury AE, Cookson MR, Reid AR, Evans IM, Hope AD et al (2004) The expression of DJ-1 (PARK7) in normal human CNS and idiopathic Parkinson's disease. *Brain* 127(2):420–430
90. Choi I, Kim J, Jeong HK, Kim B, Jou I, Park SM et al (2013) PINK1 deficiency attenuates astrocyte proliferation through mitochondrial dysfunction, reduced AKT and increased p38 MAPK activation, and downregulation of EGFR. *Glia* 61(5):800–812
91. Sanyal A, DeAndrade MP, Novis HS, Lin S, Chang J, Lengacher N et al (2020) Lysosome and inflammatory defects in GBA1-mutant astrocytes are normalized by LRRK2 inhibition. *Mov Disord* 35(5):760–773
92. Gu X-L, Long C-X, Sun L, Xie C, Lin X, Cai H (2010) Astrocytic expression of Parkinson's disease-related A53T α -synuclein causes neurodegeneration in mice. *Mol Brain* 3(1):12
93. Henry AG, Aghamohammadzadeh S, Samaroo H, Chen Y, Mou K, Needle E et al (2015) Pathogenic LRRK2 mutations, through increased kinase activity, produce enlarged lysosomes with reduced degradative capacity and increase ATP13A2 expression. *Hum Mol Genet* 24(21):6013–6028
94. Mazzulli Joseph R, Xu Y-H, Sun Y, Knight Adam L, McLean Pamela J, Caldwell Guy A et al (2011) Gaucher disease glucocerebrosidase and α -synuclein form a bidirectional pathogenic loop in synucleinopathies. *Cell* 146(1):37–52
95. Anwar S, Peters O, Millership S, Ninkina N, Doig N, Connor-Robson N et al (2011) Functional alterations to the nigrostriatal system in mice lacking all three members of the synuclein family. *J Neurosci* 31(20):7264
96. Greten-Harrison B, Polydoro M, Morimoto-Tomita M, Diao L, Williams AM, Nie EH et al (2010) $\alpha\beta\gamma$ -Synuclein triple knockout mice reveal age-dependent neuronal dysfunction. *Proc Natl Acad Sci U S A* 107(45):19573–19578
97. Hong DP, Han S, Fink AL, Uversky VN (2011) Characterization of the non-fibrillar α -synuclein oligomers. *Protein Pept Lett* 18(3):230–240
98. Nuber S, Selkoe DJ (2023) The Parkinson-associated toxin paraquat shifts physiological α -synuclein tetramers toward monomers that can be calpain-truncated and form oligomers. *Am J Pathol* 193(5):520–531
99. Konnova EA, Swanberg M (2018) Animal Models of Parkinson's Disease. In: Stoker TB, Greenland JC, editors. *Parkinson's Disease: Pathogenesis and Clinical Aspects*. Brisbane (AU): Codon Publications Copyright: The Authors; 2018
100. Singleton AB, Farrer M, Johnson J, Singleton A, Hague S, Kacher-gus J et al (2003) α -Synuclein locus triplication causes Parkinson's disease. *Science* 302(5646):841
101. Koprach JB, Kalia LV, Brotchie JM (2017) Animal models of α -synucleinopathy for Parkinson disease drug development. *Nat Rev Neurosci* 18(9):515–529
102. Delenclos M, Burgess JD, Lamprokostopoulou A, Outeiro TF, Vekrellis K, McLean PJ (2019) Cellular models of alpha-synuclein toxicity and aggregation. *J Neurochem* 150(5):566–576
103. Studer L, Vera E, Cornacchia D (2015) Programming and reprogramming cellular age in the era of induced pluripotency. *Cell Stem Cell* 16(6):591–600
104. Kara E, Crimi A, Wiedmer A, Emmenegger M, Manzoni C, Bandres-Ciga S et al (2021) An integrated genomic approach to dissect the genetic landscape regulating the cell-to-cell transfer of α -synuclein. *Cell Rep* 35(10):109189
105. El-Agnaf OM, Salem SA, Paleologou KE, Curran MD, Gibson MJ, Court JA et al (2006) Detection of oligomeric forms of alpha-synuclein protein in human plasma as a potential biomarker for Parkinson's disease. *Faseb J* 20(3):419–425
106. Cookson MR, van der Brug M (2008) Cell systems and the toxic mechanism(s) of α -synuclein. *Exp Neurol* 209(1):5–11
107. Snyder H, Mensah K, Theisler C, Lee J, Matouschek A, Wolozin B (2003) Aggregated and monomeric alpha-synuclein bind to the S6' proteasomal protein and inhibit proteasomal function. *J Biol Chem* 278(14):11753–11759
108. Lindersson E, Beedholm R, Højrup P, Moos T, Gai W, Hendil KB et al (2004) Proteasomal inhibition by alpha-synuclein filaments and oligomers. *J Biol Chem* 279(13):12924–12934
109. Lee JG, Takahama S, Zhang G, Tomarev SI, Ye Y (2016) Unconventional secretion of misfolded proteins promotes adaptation to proteasome dysfunction in mammalian cells. *Nat Cell Biol* 18(7):765–776
110. Altay MF, Liu AKL, Holton JL, Parkkinen L, Lashuel HA (2022) Prominent astrocytic alpha-synuclein pathology with unique post-translational modification signatures unveiled across Lewy body disorders. *Acta Neuropathol Commun* 10(1):163
111. Hishikawa N, Hashizume Y, Yoshida M, Sobue G (2001) Wide-spread occurrence of argyrophilic glial inclusions in Parkinson's disease. *Neuropathol Appl Neurobiol* 27(5):362–372
112. Shoji M, Harigaya Y, Sasaki A, Ueda K, Ishiguro K, Matsubara E et al (2000) Accumulation of NACP/alpha-synuclein in lewy body disease and multiple system atrophy. *J Neurol Neurosurg Psychiatry* 68(5):605–608
113. Takeda A, Hashimoto M, Mallory M, Sundsumo M, Hansen L, Masliah E (2000) C-terminal alpha-synuclein immunoreactivity in structures other than Lewy bodies in neurodegenerative disorders. *Acta Neuropathol* 99(3):296–304
114. Terada S, Ishizu H, Yokota O, Tsuchiya K, Nakashima H, Ishihara T et al (2003) Glial involvement in diffuse Lewy body disease. *Acta Neuropathol* 105(2):163–169
115. Wakabayashi K, Hayashi S, Yoshimoto M, Kudo H, Takahashi H (2000) NACP/alpha-synuclein-positive filamentous inclusions in astrocytes and oligodendrocytes of Parkinson's disease brains. *Acta Neuropathol* 99(1):14–20
116. Braak H, Sastre M, Del Tredici K (2007) Development of α -synuclein immunoreactive astrocytes in the forebrain parallels stages of intraneuronal pathology in sporadic Parkinson's disease. *Acta Neuropathol* 114(3):231–241
117. Fathy YY, Jonker AJ, Oudejans E, de Jong FJJ, van Dam AW, Rozemuller AJM et al (2019) Differential insular cortex sub-regional vulnerability to α -synuclein pathology in Parkinson's disease and dementia with Lewy bodies. *Neuropathol Appl Neurobiol* 45(3):262–277
118. Kovacs GG, Breydo L, Green R, Kis V, Puska G, Lőrincz P et al (2014) Intracellular processing of disease-associated α -synuclein in the human brain suggests prion-like cell-to-cell spread. *Neurobiol Dis* 69:76–92
119. Song YJ, Halliday GM, Holton JL, Lashley T, O'Sullivan SS, McCann H et al (2009) Degeneration in different parkinsonian syndromes relates to astrocyte type and astrocyte protein expression. *J Neuropathol Exp Neurol* 68(10):1073–1083
120. Sorrentino ZA, Goodwin MS, Riffe CJ, Dhillon JS, Xia Y, Gorion KM et al (2019) Unique α -synuclein pathology within the amygdala in Lewy body dementia: implications for disease initiation and progression. *Acta Neuropathol Commun* 7(1):142
121. Rannikko EH, Weber SS, Kahle PJ (2015) Exogenous α -synuclein induces toll-like receptor 4 dependent inflammatory responses in astrocytes. *BMC Neurosci* 16(1):57
122. Braidy N, Gai W-P, Xu YH, Sachdev P, Guillemin GJ, Jiang X-M et al (2013) Uptake and mitochondrial dysfunction of alpha-synuclein in human astrocytes, cortical neurons and fibroblasts. *Transl Neurodegen* 2(1):20

123. Castagnet PI, Golovko MY, Barceló-Coblijn GC, Nussbaum RL, Murphy EJ (2005) Fatty acid incorporation is decreased in astrocytes cultured from α -synuclein gene-ablated mice. *J Neurochem* 94(3):839–849
124. Cavaliere F, Cerf L, Dehay B, Ramos-Gonzalez P, De Giorgi F, Bourdenx M et al (2017) In vitro α -synuclein neurotoxicity and spreading among neurons and astrocytes using Lewy body extracts from Parkinson disease brains. *Neurobiol Dis* 103:101–112
125. Chen J, Yan H, Ren D-N, Yin Y, Li Z, He Q et al (2014) LRP6 dimerization through its LDLR domain is required for robust canonical Wnt pathway activation. *Cellular Signal* 26(5):1068–1074

Publisher's Note Springer Nature remains neutral with regard to jurisdictional claims in published maps and institutional affiliations.